

# Revisiting Generalization Measures Beyond IID: An Empirical Study under Distributional Shift

Sora Nakai<sup>1\*</sup> Youssef Fadhloun<sup>2\*</sup> Kacem Mathlouthi<sup>2\*</sup> Kotaro Yoshida<sup>3\*</sup>  
Ganesh Talluri<sup>4</sup> Ioannis Mitliagkas<sup>5,6</sup> Hiroki Naganuma<sup>5,6</sup>

## Abstract

Generalization remains a central yet unresolved challenge in deep learning, particularly the ability to predict a model’s performance beyond its training distribution using quantities available prior to test-time evaluation. Building on the large-scale study of Jiang et al. (2020), and concerns by Dziugaite et al. (2020), about instability across training configurations, we benchmark the robustness of generalization measures beyond IID regime. We train small-to-medium models over 10,000 hyper-parameter configurations and evaluate more than 40 measures computable from the trained model and the available training data alone. We significantly broaden the experimental scope along multiple axes: (i) extending the evaluation beyond the standard IID setting to include benchmarking for robustness across diverse distribution shifts, (ii) evaluating multiple architectures and training recipes, and (iii) newly incorporating calibration- and information-criteria-based measures to assess their alignment with both IID and OOD generalization. We find that distribution shifts can substantially alter the predictive performance of many generalization measures, while a smaller subset remains comparatively stable across settings.

## 1. Introduction

Deep learning has achieved remarkable success across various domains, ranging from computer vision (Krizhevsky et al., 2012; He et al., 2016a; Dosovitskiy et al., 2020) to natural language processing (Vaswani et al., 2017; Devlin et al.,

\*Equal contribution <sup>1</sup>Kyoto University, Kyoto, Japan <sup>2</sup>National Institute of Applied Science and Technology, Tunis, Tunisia <sup>3</sup>Institute of Science Tokyo, Tokyo, Japan <sup>4</sup>BASIS Peoria, Peoria, Arizona, USA <sup>5</sup>Mila, Montreal, Canada <sup>6</sup>Université de Montréal, Montreal, Canada. Correspondence to: Sora Nakai <nakai.sora.66n@st.kyoto-u.ac.jp>, Hiroki Naganuma <naganuma.hiroki@mila.quebec>.

2019; Brown et al., 2020). Despite these advancements, generalization—the ability of a model to maintain high performance on unseen data beyond the training set—remains a fundamental challenge (Zhang et al., 2017; Nagarajan & Kolter, 2019; Kawaguchi et al., 2022). In practical applications, the ability to accurately predict test-time performance using only information available during training is of paramount importance for ensuring the reliability and safety of deployed systems (Jiang et al., 2020; Dziugaite et al., 2020).

To address this, an extensive body of research has proposed numerous generalization measures derived from model complexity, optimization dynamics, information theory, and loss landscape. The sheer volume of these metrics has necessitated a rigorous evaluation of their reliability. A landmark study by Jiang et al. (2020); Dziugaite et al. (2020) provided a large-scale empirical survey, benchmarking 40 generalization measures using CIFAR-10 and SVHN. However, in the six years since that study, the field of deep learning has undergone significant paradigm shifts. Despite these changes, a comprehensive re-evaluation that reflects modern practical requirements is currently missing. In particular, two critical perspectives have emerged that demand urgent attention:

- i. Out-of-Distribution (OOD) Generalization: While Jiang et al. (2020) focused primarily on the Independent and Identically Distributed (IID) setting, real-world deployments frequently encounter distribution shifts (Taori et al., 2020; Koh et al., 2021). Understanding whether existing measures can predict robustness under such shifts is vital.
- ii. Confidence Calibration: For a model’s prediction to be truly trustworthy, its confidence must align with its actual accuracy (Guo et al., 2017; Krishnan & Tickoo, 2020). Recent studies have suggested a potential correlation between a model’s calibration performance and its generalization capability (Wald et al., 2021; Tada & Naganuma, 2023; Yoshida & Naganuma, 2024), yet calibration metrics are rarely treated as generalization predictors in large-scale benchmarks.

In light of these developments, this paper presents an exten-

sive benchmarking of generalization measures, including both traditional complexity-based metrics and calibration-informed indicators. We expand the scope of evaluation from standard IID settings to OOD scenarios to test the limits of these predictors. Our experimental framework involves training over 10,000 models across diverse architectures under varying hyperparameter configurations. We evaluate the reliability of each measure by observing its correlation with the train-test performance gap in both IID and OOD environments.

Our observations reveal that distribution shifts and architectural choices can substantially alter the predictive performance of many generalization measures, implying that a measure’s reliability in a specific distribution or architecture can fluctuate significantly across different settings. This underscores that no universally predictive measure exists, and exclusive reliance on specific metrics is inherently risky. In addition, we find that information criteria, calibration, and optimization-based measures, while often exhibiting negligible predictive power in IID settings, can demonstrate high predictivity in OOD scenarios. However, we also observe that this effectiveness is not static; it fluctuates or even reverses depending on the type of distribution shift and the training regime.

**Our key contributions** are as follows:

- We extend the foundational work of [Jiang et al. \(2020\)](#) by incorporating recent advancements in the field, specifically extending the evaluation to OOD settings and including calibration metrics as potential generalization indicators.
- We demonstrate that no universal generalization measure remains consistently predictive across both IID and OOD regimes, highlighting that heavy reliance on a single metric is inherently risky.
- We reveal that certain categories of measures previously considered ineffective such as information criteria, calibration, and optimization-based measures are actually more predictive in OOD scenarios than in IID settings.

## 2. Related Works

### 2.1. Generalization Measures

To Establish methodologies to accurately estimate the generalization performance of a trained model without relying on test data, various theoretical frameworks and empirical indicators have been proposed. Capacity-based measures, such as VC-dimension ([Vapnik, 1991](#); [Bartlett et al., 2019](#)), attempt to explain generalization based solely on the model architecture. However, these measures depend only on the

hypothesis space and ignore the inductive biases introduced during the training process ([Neyshabur et al., 2014](#)). In contrast, complexity-based measures focus on the properties of the learned solution. Norm-based measures operate on the hypothesis that models with smaller parameter norms tend to generalize better ([Krogh & Hertz, 1991](#); [Neyshabur et al., 2015](#); [Bartlett et al., 2017](#)). Closely related are margin-based measures, which quantify the robustness of the model by measuring the distance between data points and the decision boundary ([Bartlett et al., 2017](#); [Jiang et al., 2018](#)). Furthermore, PAC-Bayes theory provides a probabilistic framework that bounds the generalization risk by analyzing the posterior distribution of the learned parameters relative to a prior, effectively capturing the trade-off between accuracy and complexity ([Dziugaite & Roy, 2017](#)). More recently, attention has shifted towards dynamics-based and sharpness-based measures. Building on empirical observations that flat minima in the loss landscape correlate with better generalization ([Keskar et al., 2017](#); [Foret et al., 2020](#)), these metrics evaluate the local curvature of the loss function around the converged solution or analyze the gradient norms during optimization. A large-scale evaluation of these measures was conducted by [Jiang et al. \(2020\)](#). Their study revealed that while PAC-Bayes bounds and certain sharpness-based metrics showed strong correlations with generalization, traditional norm-based measures often failed to provide reliable predictions. However, their benchmarking was strictly limited to IID setting. The behavior of these measures under distribution shifts remains largely unexplored. Furthermore, their study predates several critical metrics and paradigms that have emerged recently. In this work, we address these gaps by extending the evaluation to OOD settings and incorporating these modern indicators.

### 2.2. OOD Generalization and Confidence Calibration

Standard evaluation protocols, which assume IID data, often fail to capture a model’s fragility in OOD scenarios ([Koh et al., 2021](#)). Extensive benchmarking studies, such as those using ImageNet-C ([Hendrycks & Dietterich, 2019b](#)), have demonstrated that models achieving high IID accuracy can suffer catastrophic performance drops when subjected to common corruptions or domain shifts ([Geirhos et al., 2018](#); [Recht et al., 2019](#); [Arjovsky et al., 2019](#)).

Also, the importance of confidence calibration, which measures whether a model’s predicted probabilities reflect its true correctness, has also been highlighted in recent years ([Guo et al., 2017](#)). For safety-critical applications, a model must not only be accurate but also reliable in its uncertainty estimates. However, modern deep neural networks, despite their improved accuracy, are known to be poorly calibrated and prone to overconfidence ([Guo et al., 2017](#)). Crucially, recent research suggests an intrinsic link between calibration and generalization: models that are

well-calibrated in-distribution tend to exhibit better robustness to distribution shifts (Ovadia et al., 2019; Wald et al., 2021). Despite this potential, calibration metrics (Naeini et al., 2015; Nixon et al., 2019) have rarely been evaluated as standalone predictors of generalization performance in large-scale benchmarks like that of Jiang et al. (2020). We hypothesize that these reliability metrics contain valuable signals for predicting test-time performance.

### 3. Experimental Setup

Our goal is to comprehensively evaluate how generalization measures can robustly predict test-time performance under multiple sources of environmental variation. Specifically, building upon the work of Ahuja et al. (2020), we expand the scope of generalization measures to include calibration metrics and information criteria. We validate the reliability of these measures across diverse model architectures in both IID and OOD settings, thereby enhancing comprehensiveness to better align with the demands of contemporary real-world applications.

#### 3.1. Datasets, Models, and Hyperparameters

We adopt CIFAR-10 (Krizhevsky et al., 2009), as well as PACS (Li et al., 2017) and VLCS (Fang et al., 2013) from DomainBed (Gulrajani & Lopez-Paz, 2021). To evaluate OOD performance on CIFAR-10, we employ the CIFAR-10-C and CIFAR-10-P benchmarks (Hendrycks & Dietterich, 2019a). Regarding model architectures, for CIFAR-10 experiments, we use a three-layer CNN (SimpleCNN), ResNetV2-32 (He et al., 2016b), and Network in Network (NiN) (Lin et al., 2013). For the DomainBed datasets, we adopt a ResNet-50 (He et al., 2016a) pre-trained on ImageNet-1k (Deng et al., 2009) as the feature extractor, followed by a linear classifier. All hyperparameters were swept on grids; the detailed sweep spaces are provided in the Appendix B.

#### 3.2. Training Protocol

For CIFAR-10 suites, each run is trained for 100 epochs. Optimizers and batch sizes also belong to the sweep targets here. For DomainBed suites, all models are trained using Empirical Risk Minimization (ERM) (Vapnik, 1991) with Adam (Kingma & Ba, 2015). Each run is trained for 5,000 steps with a batch size of 32 per domain.

#### 3.3. Generalization Measures

We classify generalization measures into six categories, partially adopting the taxonomy of Jiang et al. (2020).

**Baseline & Output-based Measures.** This category comprises structural capacity proxies and simple statistics of the

predictive distribution that do not require gradient or optimization information. These serve as baselines reflecting architectural scale or output-shape properties. Representative metrics include VC-dimension approximations, total parameter counts, and output statistics such as cross-entropy or negative entropy.

**Norm & Margin-based Measures.** These measures capture the geometric properties of the learned function by combining decision boundary separation with parameter complexity. This family includes metrics quantifying the classifier margin, such as the inverse logit margin, as well as various measures of scale, such as parameter  $\ell_2$  norms, spectral norms, and distances from initialization.

**Sharpness-based Measures.** Sharpness metrics quantify the sensitivity of the empirical loss to perturbations around the learned parameters, operationalizing the concept of local minima flatness. This category encompasses worst-case loss increases under structured perturbations, curvature approximations like the Hessian top eigenvalue, and PAC-Bayes bounds that interpret stability under stochastic perturbations (Foret et al., 2020).

**Optimization-based Measures.** These measures summarize the properties of gradients to capture training dynamics, stability, and local sensitivity. Unlike static baselines, these metrics explicitly leverage differential information. Examples include the variance of parameter gradients, which reflects the stochasticity of the training process, and the norms of gradients with respect to parameters or inputs.

While the four aforementioned categories were included in the experiments of Jiang et al. (2020); Dziugaite et al. (2020), we incorporate the following two categories to facilitate a more comprehensive evaluation across diverse settings:

**Information Criteria.** Information criteria balance goodness-of-fit with complexity corrections. This family includes classical criteria like AIC, as well as measures adapted for deep learning that account for posterior variability or local geometry, such as WAIC and TIC. These metrics penalize the model’s negative log-likelihood by terms reflecting effective complexity.

**Calibration & Confidence.** Finally, we include measures that evaluate the alignment between predicted probabilities and empirical accuracy. This category focuses on the reliability of the model’s uncertainty estimates, employing metrics such as Expected Calibration Error, Maximum Calibration Error, and adaptive binning variants.

More detailed descriptions of the metrics are provided in Appendix A.

### 3.4. Evaluation Protocol

We define the target metrics for measuring correlation as follows. For the CIFAR-10 suite, we adopt the generalization gap, defined as the difference between the training accuracy and the test accuracy. Specifically, we denote the gap on the standard test set as GenGap\_CIFAR10. For OOD scenarios, we define GenGap\_CIFAR10\_C and GenGap\_CIFAR10\_P as the difference between the training accuracy on CIFAR-10 and the test accuracy on CIFAR-10-C and CIFAR-10-P, respectively. For the DomainBed suite, we utilize two gaps: the difference between training and test accuracy within the training domains, and the difference between training accuracy on the source domains and test accuracy on the unseen target domain.

For correlation, which is by far the most important measure in this paper, we follow the evaluation philosophy of [Jiang et al. \(2020\)](#), and use the following two indicators.

**(i) Granulated Score  $\Psi$ .** To test whether a measure remains predictive when only a single hyperparameter axis varies, we construct subspaces in which one hyperparameter is varied while all other hyperparameters are held fixed. Within each subspace, we compute Kendall’s rank correlation  $\tau$  between a measure  $\mu$  and a target metric  $g$  as follows:

$$\tau = \frac{1}{N(N-1)/2} \sum_{1 \leq i < j \leq N} \text{sign}(\mu_i - \mu_j) \text{sign}(g_i - g_j), \quad (1)$$

where  $N$  is the number of runs in the subspace. Ties are treated as  $\text{sign}(0) = 0$  and therefore contribute zero; we do not apply tie corrections. We set the minimum subspace size to 2. Finally, we aggregate these subspace-level correlations by averaging to yield the granulated score  $\Psi$ . In addition, within each subspace with all hyperparameters except the random seed fixed, we compute  $\tau$  separately for each seed.

**(ii) Sign-error Distributions.** Following the philosophy of [Dziugaite et al. \(2020\)](#) which says that the robustness of generalization measures under various environmental shifts is important, we inspect the distributions of sign-error values in which one hyperparameter is varied. We define a hyperparameter combo as a unique assignment over selected hyperparameters excluding seed, and an environment as a pair of combos  $(h_1, h_2)$  that differ in exactly one hyperparameter. For each environment, we compute pairwise sign-error between  $g$  and  $\mu$ ,

$$\ell_{ij} = \frac{1 - \text{sign}(\mu_i - \mu_j) \text{sign}(g_i - g_j)}{2}, \quad (2)$$

optionally weight pairs by a Hoeffding-based weight  $w_{ij}$ , filter environments with effective sample size

$$n_{\text{eff}} = \frac{(\sum w_{ij})^2}{\sum w_{ij}^2} \quad (3)$$

below a threshold, and estimate the environment-level sign-error as

$$\widehat{\text{SE}} = \frac{\sum w_{ij} \ell_{ij}}{\sum w_{ij}}. \quad (4)$$

## 4. Results

### 4.1. Category-level Trends Across Models

Initially, we evaluate the summarized Granulated Kendall’s  $\tau$  correlation coefficients within each category, as depicted in Fig. 1. The figure presents a comparative analysis of across-model correlations for IID versus OOD performance. Furthermore, the proportion of data points falling into each quadrant is reported in percentiles, characterizing the global behavior of the measures.

**Baseline & Output-based Measures.** Figure 1a shows that many Baseline & Output-based measures do not preserve the sign of their correlation from IID to OOD. A substantial fraction of points fall into quadrants indicating opposite signs across regimes. This visual pattern suggests that, at a coarse level, the direction in which these measures track the generalization gap is often sensitive to distribution shift.

**Norm & Margin-based Measures.** In Figure 1b, a large portion of measures exhibit negative correlations in both IID and OOD. Visually, many points lie in the quadrant corresponding to negative-negative sign agreement, and the subset showing positive correlation appears comparatively limited and/or weak in magnitude. Taken at face value, the category as a whole does not show a strong tendency to align positively with the generalization gap across regimes. This picture is consistent with the broader observation in [Jiang et al. \(2020\)](#) that many norm-based measures can perform poorly and even correlate negatively with generalization in large hyperparameter sweeps. The scatter-plots here reinforce that, even when extending evaluation beyond IID, negative associations remain prevalent for this family, making it difficult to argue that Norm & Margin measures as a category robustly track generalization gap magnitude across regimes.

**Sharpness-based Measures.** As shown in Figure 1c, numerous measures demonstrate positive correlations across both IID and OOD scenarios. Interestingly, OOD correlations frequently exceed those in IID, implying that sharpness-related quantities gain predictive power under distribution shift. Moreover, the sign of association remains more consistent for sharpness-based measures compared to other categories. This consistency extends the findings of [Jiang et al. \(2020\)](#) to OOD environments, confirming that sharpness variants are robust candidates for generalization

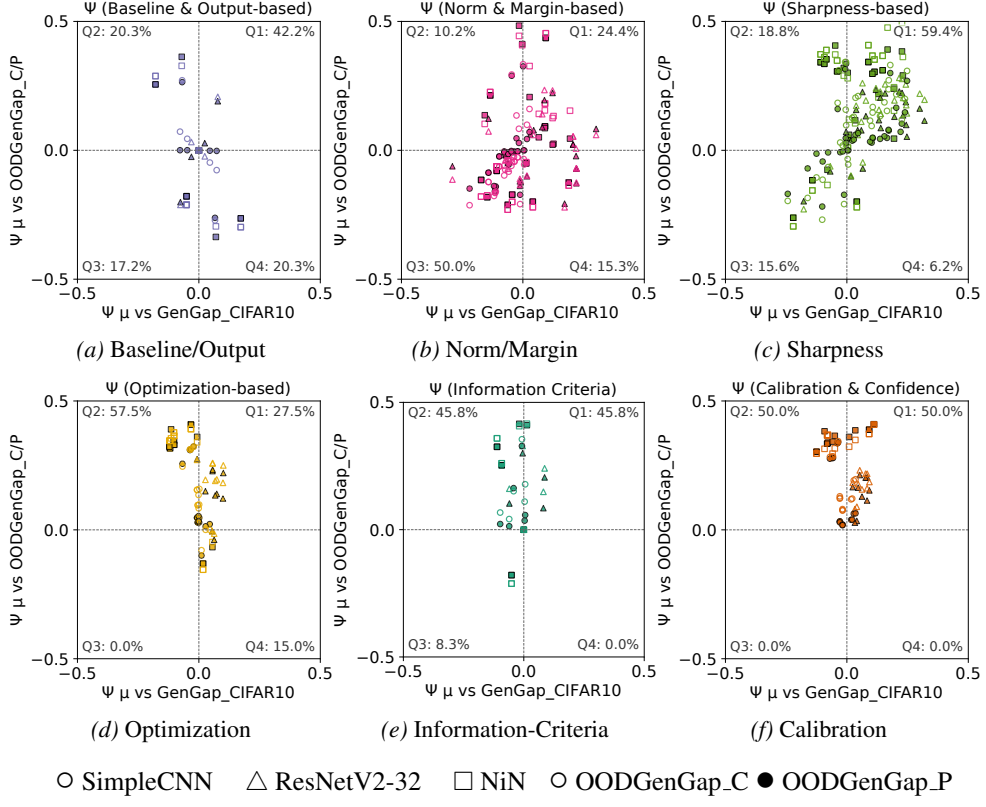


**Figure 1. Relationship between IID generalization-gap correlation and OOD generalization-gap correlation on CIFAR-10 suits.**  
Each figure shows a different measure family.

analysis.

**High Correlation in OOD but not in IID.** Figures 1d–1f reveal a shared pattern across several categories, Optimization-based, Information Criteria, and Calibration & Confidence: in the OOD regime, most measures exhibit positive correlations with the generalization gap, whereas in the IID regime the signs are mixed and the correlations are visually small in magnitude. This indicates that these families become more consistently aligned with generalization-gap variation under distribution shift than under IID settings. This regime asymmetry implies that these measures, viewed as a category-level signal, are suboptimal for driving IID generalization improvements but remain highly potent in the OOD regime.

#### 4.2. Hyperparameter-Axis Robustness Within Models

We next examine the sign-error values to determine if a measure remains predictive of the generalization gap when varying hyperparameters individually while holding all other factors constant. Figure 2 illustrates the sign-error distributions for a representative model in the IID setting and under corruption shift. In addition to the mean (orange dashed line), we report the maximum (green solid line) and the 90th percentile (pink dashed line) to expose potential heavy-tail

failure modes. The maximum and 90th percentile shows the worst case scenarios. For inspecting the robustness of measures, we look at difference of 90th percentile for each measure. Regarding hyperparameter axes, in this subsection, we focus on learning-rate and weight-decay axes.

**Learning rate.** Along the learning-rate axis, most measures exhibit substantial sign-error in both IID and corruption-shift settings, indicating that they often fail to reliably track generalization-gap magnitude when optimization dynamics are perturbed lr. That said, a small subset of measures, particularly those in the Calibration & Confidence, Sharpness-based, and Optimization-based categories, shows comparatively smaller 90th percentile sign-error than the bulk of measures in the IID setting. Under corruption shift, the relatively better-performing subset is concentrated mainly in the Sharpness-based and Optimization-based categories.

**Weight decay.** In contrast, the weight-decay axis exhibits clearer separation between categories. In the IID setting, many Norm & Margin-based and Sharpness-based measures achieve lower sign-error overall and also lower 90th percentile sign-error compared to other categories, suggesting that they are comparatively more robust predictors

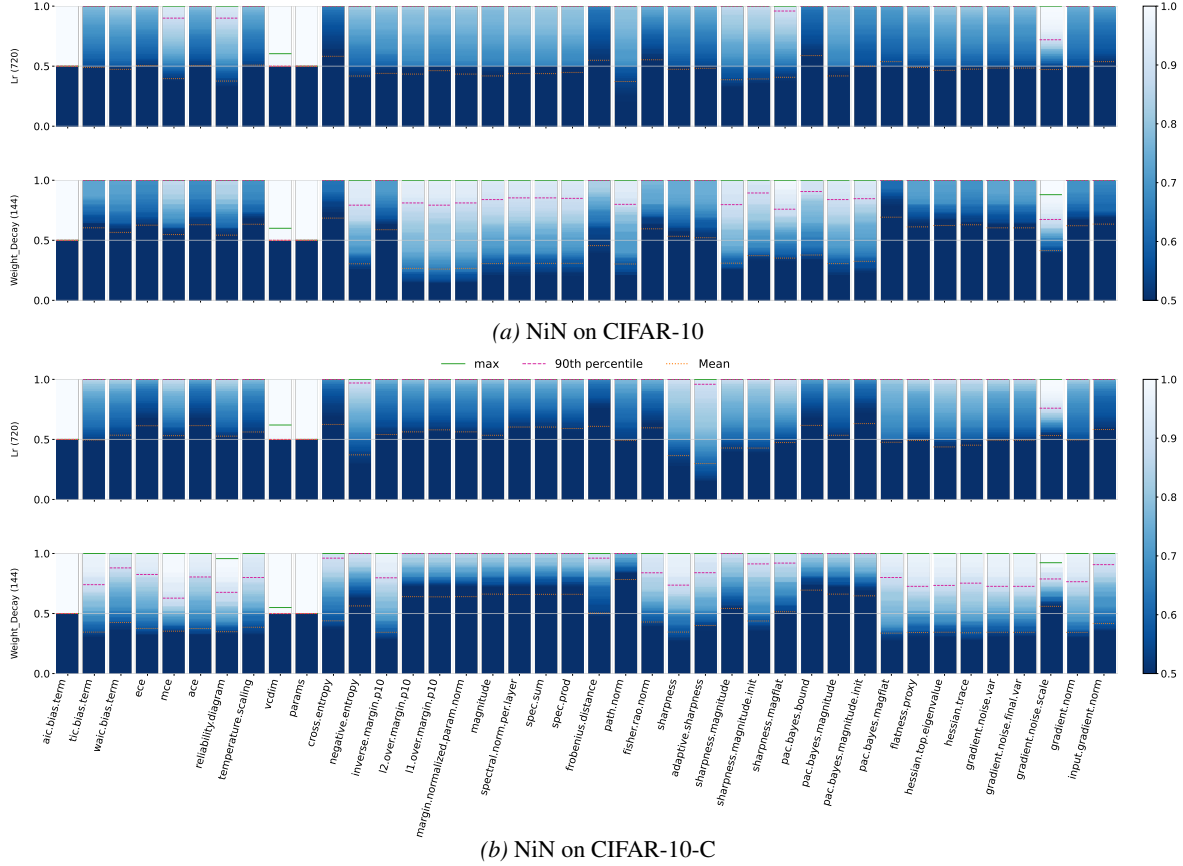


**Figure 2. Sign-error distribution of NiN on CIFAR-10 suites.** Figure 2a corresponds to the IID setting, and Figure 2b corresponds to CIFAR-10-C.

when only weight\_decay is varied. Under corruption shift, the set of comparatively robust categories changes. Measures in Information Criteria, Calibration & Confidence, and Optimization-based categories tend to achieve relatively lower 90th percentile sign-error. Several Sharpness-based measures remain among the better-performing set in both IID and OOD regimes.

### 4.3. DomainBed

This setting differs from CIFAR-10 in three respects: (i) distribution shifts arise from natural domain differences rather than synthetic corruptions and (ii) models are fine-tuned from pre-trained features rather than trained from scratch.

**Sharpness and optimization measures dominate, but with reversed sign.** Consistent with CIFAR-10, sharpness-based and optimization-based measures emerge as the strongest predictors of OOD generalization gap in both VLCS and PACS (Figures 3c and 3d). However, a striking difference emerges in the direction of correlation. In CIFAR-10-C/P, sharpness-based measures showed positive

correlations (higher sharpness associated with larger generalization gap), consistent with the flat minima hypothesis. In DomainBed, these same measures show negative correlations—higher sharpness is associated with smaller generalization gaps. This suggests that the widely-held intuition that flatter minima generalize better may not hold universally. The same reversal occurs for optimization-based measures.

**Baseline measures remain uninformative.** As in CIFAR-10, Figure 3a shows that capacity proxies exhibit zero correlation with generalization gap, confirming that architectural complexity alone does not predict OOD performance regardless of shift type.

**Calibration measures are weaker predictors.** Unlike in CIFAR-10-C/P where calibration measures showed moderate positive correlations, Figure 3f reveals that calibration metrics do not appear among the top predictors in either VLCS or PACS. This suggests that the calibration-generalization relationship may be weaker under natural domain shifts than under synthetic corruptions.

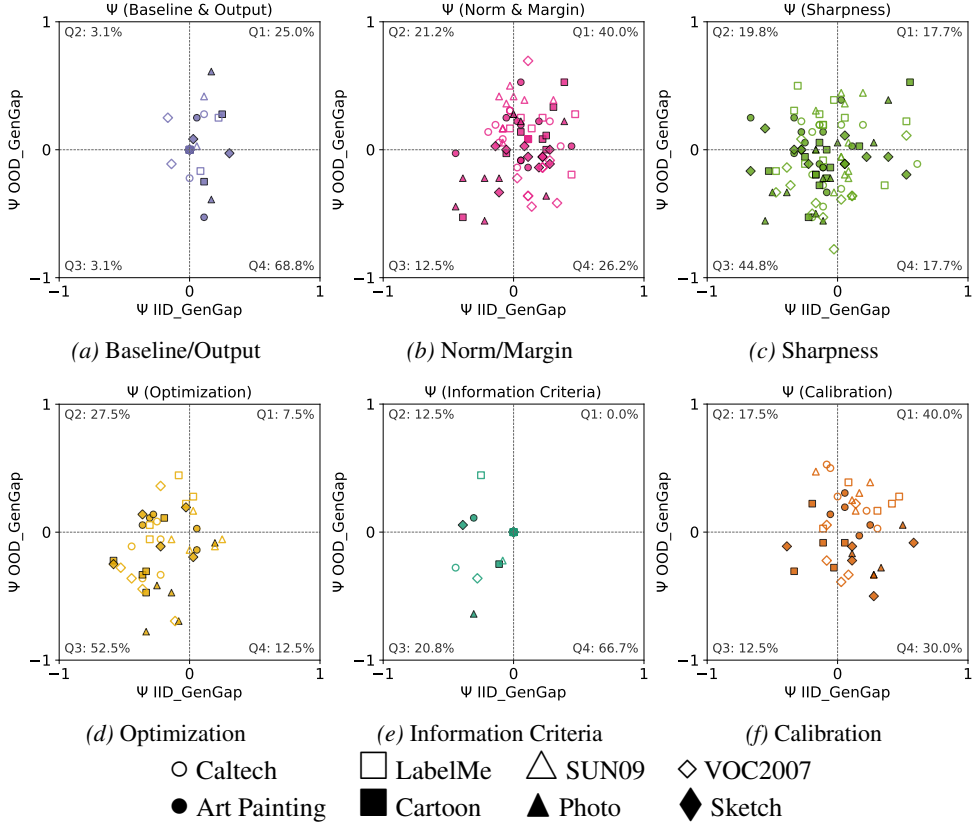


Figure 3. VLCS & PACS: Relationship between IID and OOD generalization-gap sensitivity ( $\Psi$ ). Each panel shows a different measure family.

## 5. Discussion

### 5.1. Robustness as a first-class criterion

A common practice in the literature is to identify “top” measures by their peak correlation with IID generalization. Our experiments suggest that this can be misleading for model selection in realistic settings: measures that score highly in one architecture/regime often become weak or even reverse sign under a different architecture or under shift. This motivates to recognize that no universal generalization measure exists that guarantees reliability across all contexts. Consequently, pinning model selection on a single proxy is inherently risky, as it exposes the process to the specific biases and blind spots of that individual measure. A far safer and more robust approach is to diversify the evaluation criteria by relying on a spectrum of distinct measures, thereby mitigating the impact of any single measure’s failure and ensuring that deployment decisions remain valid even under architectural changes or distribution shifts.

### 5.2. The paradox of flatness in transfer learning

Our empirical results highlight a striking contradiction regarding sharpness-based measures. While these metrics align with the flat minima hypothesis in scratch training

scenarios (CIFAR-10), exhibiting a positive correlation with the generalization gap, they display a reversed, negative correlation in the fine-tuning regime (DomainBed). This suggests that the heuristic that a flat is better (Keskar et al., 2017; Foret et al., 2020) is not universal but strictly dependent on the training paradigm. A plausible explanation is that pre-trained models already reside within a generalized, flat manifold of the loss landscape. In this context, effective adaptation to a specific target domain might require converging to a sharper, more specialized local minimum within that broader basin (Dinh et al., 2017). Consequently, future work should consider relative flatness measures that account for the geometric properties of the pre-trained initialization, rather than relying solely on absolute sharpness.

### 5.3. Optimization dynamics as robustness indicators

We observed a distinct regime asymmetry in optimization-based measures, where they serve as weak predictors for IID performance but become strong indicators of OOD generalization. This discrepancy suggests that optimization metrics capture the extent of exploration and trajectory stability, qualities that are less critical for IID memorization but vital for robustness against distribution shifts. This implies that optimization-based measures should be re-evaluated

not merely as predictors of test accuracy, but as specialized early warning signals for assessing a model’s safety and robustness in non-stationary deployment environments (McCandlish et al., 2018).

## 6. Limitations and future work

Our study has several limitations. First, our experiments are conducted on comparatively small-to-medium scale models to allow for extensive hyperparameter exploration within a limited computational budget, so it remains unclear how well the observed relationships between generalization measures and performance transfer to modern, large transformer architectures. Second, our analysis is fundamentally correlational: rank correlations can highlight associations, but they do not by themselves establish causal links, and may reflect shared confounders rather than mechanistic drivers.

A natural direction for future work is to extend the empirical evaluation to contemporary large models and training setups. On the analysis side, integrating controlled-intervention designs (e.g., fixing training error and applying single-factor perturbations) and complementing rank correlation with conditional dependence analyses could help disentangle spurious relationships from signals that are more plausibly causal. To address this, in Appendix C.2, we calculated Conditional Mutual Information (CMI) for a limited set of cases to conduct an analysis that better reflects causal relationships.

## 7. Conclusion

Our large-scale empirical study, covering over 10,000 model configurations, reveals that the predictive validity of generalization measures is highly sensitive to distribution shifts. The most critical finding of this work is that a measure’s reliability in the IID setting does not guarantee its robustness in OOD scenarios. Consequently, relying on specific measures that appear successful in IID settings poses inherent risks for practical applications. Furthermore, we confirmed that measures based on calibration, information criteria, and optimization dynamics, which often possess negligible predictive power in IID settings, can exhibit strong correlations in OOD scenarios. This implies that metrics previously dismissed due to poor IID correlation may actually hold high predictivity from the perspective of OOD generalization.

## Impact Statement

This paper presents work whose goal is to advance the field of machine learning. There are many potential societal consequences of our work, none of which we feel must be specifically highlighted here.

## Acknowledgments

This work was supported by RBC Borealis through the RBC Borealis AI Global Fellowship Award, which was awarded to Hiroki Naganuma. This work was partly achieved through the use of SQUID at D3 Center, The University of Osaka. We are also profoundly grateful to The Masason Foundation for their generous support in providing computational resources and for fostering an environment that encourages deep research collaboration.

## References

Ahuja, K., Wang, J., Dhurandhar, A., Shanmugam, K., and Varshney, K. R. Empirical or invariant risk minimization? a sample complexity perspective. *arXiv preprint arXiv:2010.16412*, 2020.

Akaike, H. A new look at the statistical model identification. *IEEE Transactions on Automatic Control*, 19(6):716–723, 1974. doi: 10.1109/TAC.1974.1100705.

Amari, S. Natural gradient works efficiently in learning. *Neural computation*, 10(2):251–276, 1998.

Arjovsky, M., Bottou, L., Gulrajani, I., and Lopez-Paz, D. Invariant risk minimization. *arXiv preprint arXiv:1907.02893*, 2019.

Bartlett, P. L., Foster, D. J., and Telgarsky, M. J. Spectrally-normalized margin bounds for neural networks. *Advances in neural information processing systems*, 30, 2017.

Bartlett, P. L., Harvey, N., Liaw, C., and Mehrabian, A. Nearly-tight vc-dimension and pseudodimension bounds for piecewise linear neural networks. *Journal of Machine Learning Research*, 20(63):1–17, 2019.

Brown, T., Mann, B., Ryder, N., Subbiah, M., Kaplan, J. D., Dhariwal, P., Neelakantan, A., Shyam, P., Sastry, G., Askell, A., et al. Language models are few-shot learners. *Advances in neural information processing systems*, 33: 1877–1901, 2020.

Cha, J., Chun, S., Lee, K., Cho, H.-C., Park, S., Lee, Y., and Park, S. Swad: Domain generalization by seeking flat minima. *Advances in Neural Information Processing Systems*, 34, 2021.

Deng, J., Dong, W., Socher, R., Li, L.-J., Li, K., and Fei-Fei, L. Imagenet: A large-scale hierarchical image

database. In *2009 IEEE Conference on Computer Vision and Pattern Recognition*, pp. 248–255, 2009. doi: 10.1109/CVPR.2009.5206848.

Devlin, J., Chang, M.-W., Lee, K., and Toutanova, K. Bert: Pre-training of deep bidirectional transformers for language understanding. In *Proceedings of the 2019 conference of the North American chapter of the association for computational linguistics: human language technologies, volume 1 (long and short papers)*, pp. 4171–4186, 2019.

Dinh, L., Pascanu, R., Bengio, S., and Bengio, Y. Sharp minima can generalize for deep nets. In *International Conference on Machine Learning*, pp. 1019–1028. PMLR, 2017.

Dosovitskiy, A., Beyer, L., Kolesnikov, A., Weissenborn, D., Zhai, X., Unterthiner, T., Dehghani, M., Minderer, M., Heigold, G., Gelly, S., et al. An image is worth 16x16 words: Transformers for image recognition at scale. *arXiv preprint arXiv:2010.11929*, 2020.

Dziugaite, G. K. and Roy, D. M. Computing nonvacuous generalization bounds for deep (stochastic) neural networks with many more parameters than training data. In *Proceedings of the 33rd Annual Conference on Uncertainty in Artificial Intelligence (UAI)*, 2017.

Dziugaite, G. K., Drouin, A., Neal, B., Rajkumar, N., Caballero, E., Wang, L., Mitliagkas, I., and Roy, D. M. In search of robust measures of generalization. *Advances in Neural Information Processing Systems*, 33:11723–11733, 2020.

Fang, C., Xu, Y., and Rockmore, D. N. Unbiased metric learning: On the utilization of multiple datasets and web images for softening bias. In *Proceedings of the IEEE International Conference on Computer Vision*, pp. 1657–1664, 2013.

Foret, P., Kleiner, A., Mobahi, H., and Neyshabur, B. Sharpness-aware minimization for efficiently improving generalization. *arXiv preprint arXiv:2010.01412*, 2020.

Geirhos, R., Rubisch, P., Michaelis, C., Bethge, M., Wichmann, F. A., and Brendel, W. Imagenet-trained cnns are biased towards texture; increasing shape bias improves accuracy and robustness. In *International conference on learning representations*, 2018.

Gulrajani, I. and Lopez-Paz, D. In search of lost domain generalization. In *International Conference on Learning Representations*, 2021.

Guo, C., Pleiss, G., Sun, Y., and Weinberger, K. Q. On calibration of modern neural networks. In *International conference on machine learning*, pp. 1321–1330. PMLR, 2017.

He, H., Huang, G., and Yuan, Y. Asymmetric valleys: Beyond sharp and flat local minima. *Advances in Neural Information Processing Systems*, 32:2553–2564, 2019.

He, K., Zhang, X., Ren, S., and Sun, J. Deep residual learning for image recognition. In *Proceedings of the IEEE conference on computer vision and pattern recognition*, pp. 770–778, 2016a.

He, K., Zhang, X., Ren, S., and Sun, J. Identity mappings in deep residual networks. In *European conference on computer vision*, pp. 630–645. Springer, 2016b.

Hendrycks, D. and Dietterich, T. Benchmarking neural network robustness to common corruptions and perturbations. In *International Conference on Learning Representations*, 2019a.

Hendrycks, D. and Dietterich, T. Benchmarking neural network robustness to common corruptions and perturbations. *Proceedings of the International Conference on Learning Representations*, 2019b.

Izmailov, P., Podoprikin, D., Garipov, T., Vetrov, D., and Wilson, A. G. Averaging weights leads to wider optima and better generalization. *arXiv preprint arXiv:1803.05407*, 2018.

Jiang, Y., Krishnan, D., Mobahi, H., and Bengio, S. Predicting the generalization gap in deep networks with margin distributions. In *International Conference on Learning Representations*, 2018.

Jiang, Y., Neyshabur, B., Mobahi, H., Krishnan, D., and Bengio, S. Fantastic generalization measures and where to find them. In *International Conference on Learning Representations*, 2020.

Kawaguchi, K., Kaelbling, L. P., and Bengio, Y. Generalization in deep learning. In *Mathematical Aspects of Deep Learning*. Cambridge University Press, 2022. doi: 10.1017/9781009025096.003.

Keskar, N. S., Dheevatsa Mudigere, J. N., Smelyanskiy, M., and Tang, P. T. P. On large-batch training for deep learning: Generalization gap and sharp minima. In *International Conference on Learning Representations*, 2017.

Kingma, D. P. and Ba, J. Adam: A method for stochastic optimization. In *International Conference on Learning Representations (ICLR)*, 2015. URL <https://arxiv.org/abs/1412.6980>.

Koh, P. W., Sagawa, S., Marklund, H., Xie, S. M., Zhang, M., Balsubramani, A., Hu, W., Yasunaga, M., Phillips, R. L., Gao, I., et al. Wilds: A benchmark of in-the-wild distribution shifts. In *International Conference on Machine Learning*, pp. 5637–5664. PMLR, 2021.

Krishnan, R. and Tickoo, O. Improving model calibration with accuracy versus uncertainty optimization. *Advances in Neural Information Processing Systems*, 33:18237–18248, 2020.

Krizhevsky, A., Nair, V., and Hinton, G. Cifar-10 and cifar-100 (canadian institute for advanced research). <http://www.cs.toronto.edu/~kriz/cifar.html>, 2009. MIT License.

Krizhevsky, A., Sutskever, I., and Hinton, G. E. Imagenet classification with deep convolutional neural networks. *Advances in neural information processing systems*, 25, 2012.

Krogh, A. and Hertz, J. A simple weight decay can improve generalization. *Advances in neural information processing systems*, 4, 1991.

Li, D., Yang, Y., Song, Y.-Z., and Hospedales, T. M. Deeper, broader and artier domain generalization. In *Proceedings of the IEEE international conference on computer vision*, pp. 5542–5550, 2017.

Lin, M., Chen, Q., and Yan, S. Network in network. *arXiv preprint arXiv:1312.4400*, 2013.

McCandlish, S., Kaplan, J., Amodei, D., and Team, O. D. An empirical model of large-batch training. *arXiv preprint arXiv:1812.06162*, 2018.

Naeini, M. P., Cooper, G., and Hauskrecht, M. Obtaining well calibrated probabilities using bayesian binning, 2015.

Nagarajan, V. and Kolter, J. Z. Uniform convergence may be unable to explain generalization in deep learning. *Advances in Neural Information Processing Systems*, 32, 2019.

Neyshabur, B., Tomioka, R., and Srebro, N. In search of the real inductive bias: On the role of implicit regularization in deep learning. *CoRR*, abs/1412.6614, 2014. URL <https://api.semanticscholar.org/CorpusID:6021932>.

Neyshabur, B., Tomioka, R., and Srebro, N. Norm-based capacity control in neural networks. In *Conference on learning theory*, pp. 1376–1401. PMLR, 2015.

Nixon, J., Dusenberry, M. W., Zhang, L., Jerfel, G., and Tran, D. Measuring calibration in deep learning. In *CVPR workshops*, volume 2, 2019.

Ovadia, Y., Fertig, E., Ren, J., Nado, Z., Sculley, D., Nowozin, S., Dillon, J., Lakshminarayanan, B., and Snoek, J. Can you trust your model’s uncertainty? evaluating predictive uncertainty under dataset shift. *Advances in neural information processing systems*, 32, 2019.

Recht, B., Roelofs, R., Schmidt, L., and Shankar, V. Do imagenet classifiers generalize to imagenet? In *International conference on machine learning*, pp. 5389–5400. PMLR, 2019.

Shallue, C. J., Lee, J., Antognini, J., Sohl-Dickstein, J., Frostig, R., and Dahl, G. E. Measuring the effects of data parallelism on neural network training. *Journal of Machine Learning Research*, 20(112):1–49, 2019.

Tada, K. and Naganuma, H. How image corruption and perturbation affect out-of-distribution generalization and calibration. In *2023 International Joint Conference on Neural Networks (IJCNN)*, pp. 1–6, 2023. doi: 10.1109/IJCNN54540.2023.10191806.

Takeuchi, K. Distribution of information statistics and validity criteria of models. *Mathematical Science*, 153:12–18, 1976.

Taori, R., Dave, A., Shankar, V., Carlini, N., Recht, B., and Schmidt, L. Measuring robustness to natural distribution shifts in image classification. *arXiv preprint arXiv:2007.00644*, 2020.

Vapnik, V. Principles of risk minimization for learning theory. *Advances in neural information processing systems*, 4, 1991.

Vaswani, A., Shazeer, N., Parmar, N., Uszkoreit, J., Jones, L., Gomez, A. N., Kaiser, Ł., and Polosukhin, I. Attention is all you need. *Advances in neural information processing systems*, 30, 2017.

Wald, Y., Feder, A., Greenfeld, D., and Shalit, U. On calibration and out-of-domain generalization. *Advances in neural information processing systems*, 34:2215–2227, 2021.

Watanabe, S. and Opper, M. Asymptotic equivalence of bayes cross validation and widely applicable information criterion in singular learning theory. *Journal of machine learning research*, 11(12), 2010.

Yoshida, K. and Naganuma, H. Towards understanding variants of invariant risk minimization through the lens of calibration, 2024.

Zhang, C., Bengio, S., Hardt, M., Recht, B., and Vinyals, O. Understanding deep learning requires rethinking generalization. In *International Conference on Learning Representations*, 2017. URL <https://arxiv.org/abs/1611.03530>.

Zhang, G., Li, L., Nado, Z., Martens, J., Sachdeva, S., Dahl, G. E., Shallue, C. J., and Grosse, R. Which algorithmic choices matter at which batch sizes? insights from a noisy quadratic model. *arXiv preprint arXiv:1907.04164*, 2019.

## A. More Details on Generalization Measures

Table 1. Summary of Generalization Measures evaluated in this study. The measures are categorized into six groups based on their theoretical properties.

Measure Name	Description
<b>Baseline &amp; Output-based Measures</b>	
vcdim	Approximate VC-dimension bound based on network depth and width.
params	Total number of trainable model parameters.
magnitude	The $\ell_2$ norm of the parameter vector.
cross_entropy	Average cross-entropy loss on the training set (or evaluation split).
negative_entropy	Negative entropy of the predictive distribution (measure of confidence/peakiness).
<b>Margin &amp; Norm-based Measures</b>	
inverse_margin_p10	Inverse of the 10th percentile of the logical margin distribution.
l2_over_margin_p10	Ratio of parameter $\ell_2$ norm to the 10th percentile margin.
l1_over_margin_p10	Ratio of parameter $\ell_1$ norm to the 10th percentile margin.
margin_normalized_param_norm	Parameter norms scaled by the robust margin.
spectral_norm_per_layer	Sum of spectral norms computed per layer.
spec_sum	Sum of the spectral norms of the weight matrices.
spec_prod	Product of the spectral norms of the weight matrices.
frobenius_distance	Frobenius distance between the final weights and initialization.
path_norm	Path-norm; a scale-invariant capacity measure.
fisher_rao_norm	Fisher-Rao norm; geometry-aware norm based on the Fisher Information Matrix.
<b>Sharpness-based Measures</b>	
sharpness	Worst-case loss increase within a neighborhood (standard definition).
adaptive_sharpness	Sharpness measured with an adaptive neighborhood size.
sharpness_magnitude	Sharpness scaled by the magnitude of the parameters.
sharpness_magnitude_init	Sharpness scaled by the magnitude relative to initialization.
sharpness_magflat	Flatness measure using multiplicative perturbations proportional to weight magnitude.
pac_bayes_bound	PAC-Bayes generalization bound (interpreted as stability/flatness).
pac_bayes_magnitude	PAC-Bayes bound incorporating parameter magnitude.
pac_bayes_magnitude_init	PAC-Bayes bound incorporating distance from initialization.
pac_bayes_magflat	PAC-Bayes variant related to magnitude-proportional flatness.
flatness_proxy	Flatness proxy based on Elastic Weight Consolidation (EWC).
hessian_top_eigenvalue	The largest eigenvalue of the Hessian matrix (worst-case curvature).
hessian_trace	The trace of the Hessian matrix (average curvature).
<b>Optimization-based Measures</b>	
gradient_noise_var	Variance of the stochastic gradients during training.
gradient_noise_final_var	Variance of the gradients measured at the final solution.
gradient_noise_scale	Ratio of gradient noise variance to the mean squared gradient norm.
gradient_norm	Aggregate norm of the gradients across minibatches.
input_gradient_norm	Norm of the gradient of the loss with respect to the input (sensitivity).

Continued on next page

**Table 1 – continued from previous page**

Metric Name	Description
<b>Information Criteria</b>	
aic_bias_term	The complexity penalty term of AIC (based on parameter count).
tic_bias_term	The complexity penalty term of TIC (trace term).
waic_bias_term	The complexity penalty term of WAIC (log-likelihood variance).
<b>Calibration &amp; Confidence</b>	
ece	Expected Calibration Error; weighted average difference between confidence and accuracy in bins.
mce	Maximum Calibration Error; the maximum gap between confidence and accuracy across bins.
ace	Adaptive Calibration Error; uses adaptive binning based on quantiles.
reliability_diagram	Calibration error derived from bin-wise reliability diagrams.
temperature_scaling	Calibration error calculated after post-hoc optimal temperature scaling.

Table 1 presents a list of generalization measures adopted in this study. The measures newly validated in this paper, in addition to those in Jiang et al. (2020), are described below.

### A.1. Baseline & Output-based Measures

**vcdim.** We report an architecture-based VC-dimension proxy. Classical VC theory motivates capacity control via VC-style complexity measures (Vapnik, 1991). In our experiments, we use the standard parameter-count proxy commonly used as a simple capacity baseline in generalization-measure evaluations (Jiang et al., 2020):

$$vcdim = W \log W, \quad (5)$$

where  $W$  is the number of trainable parameters. This proxy is also consistent with known scaling behavior of VC/pseudodimension upper bounds for piecewise-linear networks (Bartlett et al., 2019). For 4D image inputs, we instead use the  $\mu_{VC}$  upper bound (Eq. 15) from *Fantastic Generalization Measures and Where to Find Them* by Jiang et al. (2020). We computed this measure to create a capacity-only baseline to test whether architecture scale alone predicts IID/OOD generalization gaps (Jiang et al., 2020; Dziugaite et al., 2020).

### A.2. Margin & Norm-based Measures

**inverse\_margin\_p10.** For each sample  $(x_n, y_n)$ , define a margin  $m_n$ . For classification runs,  $m_n$  is computed from logits; for language-modeling-style runs it is computed from log-probabilities. Margin distributions (especially lower-tail statistics) have been shown to correlate with generalization gaps and are used in practice as predictors (Jiang et al., 2018; 2020). Let  $q_{0.10}$  be the empirical 10th percentile of  $\{m_n\}_{n=1}^N$ . We compute a sign-preserving, clamped inverse:

$$\text{inverse\_margin\_p10} = \frac{1}{\text{clip}(q_{0.10}, -\epsilon, \epsilon)} \quad \text{where} \quad \text{clip}(z, -\epsilon, \epsilon) = \text{sign}(z) \max(|z|, \epsilon). \quad (6)$$

We computed this measure to create a low-tail separation/robustness signal (small-magnitude lower-tail margins  $\Rightarrow$  larger score) used as a predictor of generalization gaps (Jiang et al., 2018; Bartlett et al., 2017).

**l2\_over\_margin\_p10.** This measure is an alias of `margin_normalized_param_norm` under default settings. Norm- and margin-based quantities are standard complexity surrogates for deep nets (Neyshabur et al., 2015; Bartlett et al., 2017; Jiang et al., 2020). Let  $\theta$  be the vector of all trainable parameters (including biases by default) and let  $\|\theta\|_2$  be its  $\ell_2$  norm. Let  $S$  denote the chosen lower-tail margin statistic (default: `p10`), computed from logits for classification and from log-probabilities for language-modeling-style runs. The reported value is

$$\text{l2\_over\_margin\_p10} = \frac{\|\theta\|_2}{\max(|S|, \epsilon)}. \quad (7)$$

We computed this measure to create a combined scale+tail-margin proxy to test whether larger parameter scale relative to worst-case margins correlates with poorer generalization (Neyshabur et al., 2015; Jiang et al., 2018; Bartlett et al., 2017).

**l1\_over\_margin\_p10.** Same implementation family as above, but using  $\ell_1$  norm.  $\ell_1$ -type norms appear in norm-based capacity control and can behave differently under sparsity/scale effects (Neyshabur et al., 2015; 2014):

$$\text{l1\_over\_margin\_p10} = \frac{\|\theta\|_1}{\max(|S|, \epsilon)}, \quad (8)$$

with the same  $S$  definition (default statistic  $p10$ ). We computed this measure to probe whether absolute-scale/sparsity-sensitive norms behave differently as generalization predictors under IID and shift (Jiang et al., 2020; Dziugaite et al., 2020).

**margin\_normalized\_param\_norm.** This is the canonical implementation used by `l2_over_margin_p10` by default. With  $\|\theta\|_2$  including biases and  $S$  the selected margin statistic (default  $p10$ ), we compute

$$\text{margin\_normalized\_param\_norm} = \frac{\|\theta\|_2}{\max(|S|, \epsilon)}. \quad (9)$$

We computed this measure to create a single scalar that merges parameter scale and lower-tail margin magnitude, evaluated as a candidate predictor of IID/OOD generalization gaps across architectures (Neyshabur et al., 2015; Bartlett et al., 2017; Jiang et al., 2018).

**spectral\_norm\_per\_layer.** For each layer weight tensor  $W_\ell$ , we estimate the spectral norm via power iteration on a matrix flattening of the weights. Spectral norms are central to spectrally-normalized margin bounds and Lipschitz-style capacity control for deep networks (Bartlett et al., 2017; Neyshabur et al., 2015). For convolutions, kernels are flattened (not the full convolution operator). Let  $\hat{\sigma}_\ell$  denote the resulting estimate. We aggregate to a scalar mean

$$\text{spectral\_norm\_per\_layer} = \frac{1}{L} \sum_{\ell=1}^L \hat{\sigma}_\ell. \quad (10)$$

We computed this measure to create an operator-scale proxy (approximate Lipschitz/conditioning signal) to test correlation with IID/OOD generalization gaps (Bartlett et al., 2017; Jiang et al., 2020).

**path\_norm.** This measure is implementation-dependent by model family. Path- and norm-based controls are standard complexity surrogates and appear in multiple generalization-measure catalogs (Neyshabur et al., 2014; 2015; Jiang et al., 2020). For language-modeling-style runs, we use a log-Frobenius aggregation of selected linear weights:

$$\text{path\_norm} = \sum_{\ell=1}^L \log \|W_\ell\|_F. \quad (11)$$

For convolutional models, we use a channel-wise propagation approximation rather than exact input-to-output path enumeration. We computed this measure to create a structured weight-aggregation complexity proxy (exact path norms are intractable at scale) intended to correlate with generalization behavior (Neyshabur et al., 2014; Jiang et al., 2020; Dziugaite et al., 2020).

**fisher\_rao\_norm.** Let  $p_\theta(y \mid x)$  be the predictive distribution and define  $g_n = \nabla_\theta \log p_\theta(y_n \mid x_n)$ . Fisher-information geometry motivates measuring parameter sensitivity through Fisher-metric-weighted quantities (Amari, 1998; Kawaguchi et al., 2022). The Fisher-Rao quantity is computed as

$$\text{fisher\_rao\_norm} = \sqrt{\mathbb{E} \left[ (\theta^\top g)^2 \right]} \approx \sqrt{\frac{1}{N} \sum_{n=1}^N (\theta^\top g_n)^2} = \sqrt{\theta^\top \hat{F} \theta}, \quad (12)$$

where  $\hat{F} = \frac{1}{N} \sum_{n=1}^N g_n g_n^\top$ . For language-modeling-style runs, we use a proxy based on elementwise products  $(\theta \odot \nabla_\theta \log p)^2$  consistent with the same quadratic form. We computed this measure to create an information-geometric complexity measure that weights parameters by their sensitivity in log-likelihood space (Amari, 1998; Jiang et al., 2020).

### A.3. Sharpness-based Measures

**sharpness.** Sharpness is computed in a SAM-style one-step perturbation per minibatch, then averaged over the data loader. Sharpness and sharp minima have been linked to generalization behavior (e.g., large-batch effects) (Keskar et al., 2017), and SAM operationalizes a sharpness-aware objective (Foret et al., 2020). For a batch loss  $\hat{L}_b(\theta)$ , define the normalized gradient direction

$$u_b = \frac{\nabla_{\theta} \hat{L}_b(\theta)}{\left\| \nabla_{\theta} \hat{L}_b(\theta) \right\|_2}. \quad (13)$$

The one-step perturbed parameters are

$$\theta_b^+ = \theta + \rho u_b, \quad (14)$$

and we report the average batch-wise loss increase

$$\text{sharpness} = \mathbb{E}_b \left[ \hat{L}_b(\theta_b^+) - \hat{L}_b(\theta) \right]. \quad (15)$$

We computed this measure to create a scalable flatness/sensitivity proxy (one-step) that remains informative across architectures and evaluation regimes (Foret et al., 2020; Cha et al., 2021; Izmailov et al., 2018).

**adaptive\_sharpness.** Adaptive sharpness scans over a log-spaced set of radii  $\{\rho_k\}_{k=1}^K$ , computes the SAM-style one-step sharpness at each radius, and by default returns the maximal normalized value:

$$\text{adaptive\_sharpness} = \max_{k \in \{1, \dots, K\}} \frac{\text{sharpness}(\rho_k)}{\rho_k}. \quad (16)$$

We computed this measure to create a radius-robust sharpness summary that reduces sensitivity to a single perturbation scale (Foret et al., 2020; Jiang et al., 2020; Cha et al., 2021).

**sharpness\_magnitude.** Let the baseline empirical loss be  $\hat{L}(\theta) = \frac{1}{N} \sum_{n=1}^N \text{CE}_n(\theta)$ . Magnitude-aware perturbations are commonly used in empirical generalization-measure evaluations to improve comparability across scales (Jiang et al., 2020; Dziugaite et al., 2020). For each perturbation sample  $k$ , and for each parameter tensor  $p$ , we apply additive Gaussian noise scaled by the tensor standard deviation:

$$p \leftarrow p + \epsilon, \quad \epsilon \sim \mathcal{N}(0, (r \cdot \text{std}(p))^2). \quad (17)$$

Let  $\Delta_k = \hat{L}(\theta + \Delta\theta_k) - \hat{L}(\theta)$  be the loss increase. We aggregate across samples (default: max; optionally mean):

$$\text{sharpness\_raw} = \max_k \Delta_k. \quad (18)$$

Define the magnitude factor

$$M_{\text{orig}} = \frac{\|\theta\|_2}{\sqrt{d}}, \quad (19)$$

where  $d$  is the total number of parameters. The final measure is

$$\text{sharpness\_magnitude} = \text{sharpness\_raw} \cdot M_{\text{orig}}. \quad (20)$$

We computed this measure to create a scale-aware sharpness signal that probes sensitivity of the learned solution to stochastic perturbations (Keskar et al., 2017; Jiang et al., 2020; He et al., 2019).

**sharpness\_magnitude\_init.** This measure matches `sharpness_magnitude` but uses an initialization-relative magnitude factor when an init snapshot  $\theta_0$  is available:

$$M_{\text{init}} = \frac{\|\theta - \theta_0\|_2}{\sqrt{d}}, \quad (21)$$

falling back to  $M_{\text{orig}}$  if  $\theta_0$  is unavailable. The final measure is

$$\text{sharpness\_magnitude\_init} = \text{sharpness\_raw} \cdot M_{\text{init}}. \quad (22)$$

We computed this measure to capture sharpness weighted by distance traveled during training, reducing sensitivity to raw parameter scaling (Jiang et al., 2020; Dziugaite et al., 2020; Izmailov et al., 2018).

**sharpness\_magflat.** With the same baseline loss  $\hat{L}(\theta)$ , we sample magnitude-aware perturbations

$$\Delta\theta_k = r \cdot z_k \odot (|\theta| + \epsilon_{\text{scale}}), \quad z_k \sim \mathcal{N}(0, I), \quad (23)$$

and compute loss increases  $\Delta_k = \hat{L}(\theta + \Delta\theta_k) - \hat{L}(\theta)$ . We aggregate across samples (default: max; optionally mean):

$$\text{sharpness_magflat} = \max_k \Delta_k. \quad (24)$$

We computed this measure to create a magnitude-aware flatness proxy intended to improve comparability across architectures and training scales (Jiang et al., 2020; Dziugaite et al., 2020; Keskar et al., 2017).

**pac\_bayes\_magflat.** PAC-Bayes analysis provides nonvacuous generalization bounds for deep stochastic predictors under suitable choices of priors/posteriors (Dziugaite & Roy, 2017; Dziugaite et al., 2020). We define a diagonal Gaussian posterior centered at the learned parameters with magnitude-scaled variance:

$$Q = \mathcal{N}(\theta, \text{diag}(\sigma_{q,i}^2)), \quad \sigma_{q,i}^2 = (\sigma_{\text{post}}|\theta_i|)^2, \quad (25)$$

and an isotropic Gaussian prior

$$P = \mathcal{N}(0, \sigma_{\text{prior}}^2 I). \quad (26)$$

We approximate the Gibbs empirical 0–1 risk via multiplicative noise:

$$\theta' = \theta \odot (1 + \sigma_{\text{post}}\varepsilon), \quad \varepsilon \sim \mathcal{N}(0, I), \quad \hat{R}_G = \mathbb{E}_{\theta'}[\text{empirical 0–1 error}]. \quad (27)$$

The KL divergence is

$$\text{KL}(Q\|P) = \frac{1}{2} \sum_i \left( \frac{\theta_i^2}{\sigma_p^2} + \frac{\sigma_{q,i}^2}{\sigma_p^2} - 1 - \log \frac{\sigma_{q,i}^2}{\sigma_p^2} \right), \quad \sigma_p^2 = \sigma_{\text{prior}}^2. \quad (28)$$

Using a McAllester-style bound, we report

$$\text{pac_bayes_magflat} = \hat{R}_G + \sqrt{\frac{\text{KL}(Q\|P) + \log\left(\frac{2\sqrt{n}}{\delta}\right)}{2n}}, \quad (29)$$

where  $n$  is the sample count used for the bound and  $\delta$  is the confidence parameter. We computed this measure in our experiment to see the uncertainty and scale-aware bound, which is intended to remain informative across model families and evaluation regimes (Dziugaite & Roy, 2017; Jiang et al., 2020; Dziugaite et al., 2020).

**flatness\_proxy.** We estimate the diagonal of the empirical Fisher for each parameter coordinate  $i$  using per-batch gradients:

$$F_i \approx \frac{1}{B} \sum_{b=1}^B \left( \frac{\partial L_b}{\partial w_i} \right)^2. \quad (30)$$

With prior precision  $\lambda$  (a fixed hyperparameter), define

$$\pi_i = F_i + \lambda. \quad (31)$$

We aggregate across coordinates using a configured statistic (mean/median/harmonic mean):

$$\text{flatness_proxy} = \text{agg}_i(\pi_i). \quad (32)$$

We computed this measure to create a lightweight precision proxy that approximates local sensitivity without explicit Hessian computation, consistent with flatness/curvature-focused generalization analyses (Keskar et al., 2017; Cha et al., 2021; Jiang et al., 2020).

**hessian\_top\_eigenvalue.** Using a single-batch loss  $L(\theta)$ , we estimate the largest Hessian eigenvalue via power iteration with Hessian–vector products:

$$v_{t+1} = \frac{Hv_t}{\|Hv_t\|_2}, \quad (33)$$

and report the Rayleigh quotient

$$\lambda_{\max} \approx v^\top Hv. \quad (34)$$

We computed this measure to create a direct curvature indicator capturing the dominant local curvature direction, aligning with curvature-based accounts of sharp/flat minima (Keskar et al., 2017; He et al., 2019; Jiang et al., 2020).

**hessian\_trace.** We estimate the Hessian trace using the Hutchinson estimator with Rademacher vectors  $v_s$ :

$$\text{tr}(H) \approx \frac{1}{S} \sum_{s=1}^S v_s^\top Hv_s. \quad (35)$$

We computed this measure to create a scalar summary of total curvature that complements  $\lambda_{\max}$  and is commonly used in curvature/flatness studies of generalization (Keskar et al., 2017; He et al., 2019; Jiang et al., 2020).

#### A.4. Optimization-based Measures

**gradient\_noise\_scale.** Let  $g_b$  be the per-batch gradient vector and let  $d$  denote the number of gradient coordinates. Gradient noise and batch-size effects are central to several empirical accounts of optimization dynamics and generalization (Shallue et al., 2019; Zhang et al., 2019). For each coordinate  $i$ ,

$$\bar{g}_i = \frac{1}{B} \sum_{b=1}^B g_{b,i}, \quad \text{Var}_i = \frac{1}{B} \sum_{b=1}^B (g_{b,i} - \bar{g}_i)^2. \quad (36)$$

We compute the noise scale

$$\text{gradient\_noise\_scale} = \frac{1}{d} \sum_{i=1}^d \frac{\text{Var}_i}{\bar{g}_i^2 + \epsilon}. \quad (37)$$

We computed this measure for our experiments to create a training-dynamics stability statistic that summarizes gradient stochasticity as a candidate predictor of generalization behavior (Zhang et al., 2019; Shallue et al., 2019; Keskar et al., 2017).

**gradient\_norm.** For each batch, compute the gradient of the mean loss and its global norm

$$\|g\|_2 = \left( \sum_p \|g_p\|_2^2 \right)^{1/2} \quad (\text{or } \|g\|_1, \|g\|_\infty \text{ if configured}), \quad (38)$$

then aggregate across batches using a configured statistic (mean/max/std/median):

$$\text{gradient\_norm} = \text{agg}_b(\|g^{(b)}\|). \quad (39)$$

We computed this measure to create a compact summary of the gradient scale over evaluation batches, which was used to relate optimization sensitivity to IID/OOD generalization gaps (Jiang et al., 2020; Zhang et al., 2019; Dziugaite et al., 2020).

#### A.5. Information Criteria

**aic and aic\_bias\_term.** The Akaike Information Criterion (AIC) (Akaike, 1974) is derived from maximum likelihood estimation under standard regularity conditions. It is defined as:

$$\text{AIC} = 2 \text{NLL}(\hat{\theta}) + 2k, \quad (40)$$

where  $\text{NLL}(\hat{\theta}) = -\log L(\hat{\theta})$  is the negative log-likelihood evaluated at the MLE and  $k$  is the number of parameters. In our implementation, NLL is computed as the sum over all samples. The AIC bias term quantifies model complexity to mitigate

overfitting and is given by  $2k$ . We take  $k$  to be the total number of trainable parameters. Optionally, when the sample size  $N$  is small relative to  $k$ , we use the finite-sample correction (AICc), in which case the bias term becomes

$$2k + \frac{2k(k+1)}{N-k-1}, \quad (41)$$

valid when  $N > k+1$ .

**tic, tic\_bias\_term, and tic\_bias\_term\_bound.** The Takeuchi Information Criterion (TIC) (Takeuchi, 1976) generalizes AIC by relaxing the realizability assumption. It remains valid under model misspecification (i.e., when the true distribution is not contained in the model family), provided standard regularity conditions hold. It is defined as

$$\text{TIC} = \text{NLL}_{\text{mean}}(\theta) + \text{Tr}(I(\theta)^{-1}J(\theta)), \quad (42)$$

where  $I(\theta)$  is the Fisher information based on the Hessian of the mean NLL, and  $J(\theta)$  is the empirical Fisher based on per-sample scores. When the model is correctly specified,  $J \approx I$  and the trace term reduces to the parameter count.

The TIC bias term is  $\text{Tr}(I(\theta)^{-1}J(\theta))$ . Since forming and inverting the full Fisher information matrix is infeasible at scale, we approximate the trace via a diagonal sandwich approximation:

$$\text{bias}_{\text{TIC}} = \sum_j \frac{\text{diag}(J)_j}{\text{diag}(I)_j + \epsilon}, \quad (43)$$

where  $\text{diag}(I)$  and  $\text{diag}(J)$  denote the diagonals of (respectively) the Hessian of the mean NLL (estimated via Hutchinson's method) and the empirical Fisher (estimated from per-sample gradients).

We also compute a deterministic upper bound for this diagonally approximated bias term using the inequality  $\sum_j \frac{b_j}{a_j} \leq \frac{\sum_j b_j}{\min_j a_j}$  for positive vectors  $a, b$ :

$$\text{bias}_{\text{TIC}}^{\text{bound}} = \frac{\sum_j \text{diag}(J)_j}{\max(\min_j \text{diag}(I)_j, \epsilon)}. \quad (44)$$

**waic and waic\_bias\_term.** The Widely Applicable Information Criterion (WAIC) (Watanabe & Opper, 2010) is Bayesian and grounded in singular learning theory. Unlike AIC and TIC, WAIC remains valid for singular models (e.g., neural networks and mixture models) where regularity conditions fail, and it does not require realizability. WAIC is computed from the posterior predictive distribution as

$$\text{WAIC} = -2 \text{LPPD} + 2k_{\text{WAIC}}, \quad (45)$$

where LPPD is the log pointwise predictive density and  $k_{\text{WAIC}}$  is the effective number of parameters, typically estimated via the variance of the log-likelihood under the posterior. In our runs, posterior samples are generated by MC Dropout when the dropout probability is greater than 0; when it is 0, we use weight noise.

The WAIC bias term is twice the effective number of parameters and is computed as

$$\text{bias}_{\text{WAIC}} = 2 \sum_{n=1}^N \text{Var}_{\theta \sim p(\theta|D)} [\ln p(x_n | \theta)], \quad (46)$$

where  $N$  is the number of samples and the variance is taken over posterior samples of  $\theta$ .

## A.6. Confidence-based Measures

**ece.** Expected Calibration Error (ECE) (Naeini et al., 2015) partitions model predictions into equally spaced confidence bins. It calculates the absolute difference between the average confidence and the accuracy within each bin, taking a weighted average based on the number of samples in each bin. Let  $y$  denote the ground-truth label and  $\tilde{p}$  denote the predicted probability for a given sample, with  $\tilde{y}$  representing the final predicted class. Let  $N$  be the total number of samples in the

dataset used to calculate ECE, and let  $B_m$  be the set of samples falling into the  $m$ -th confidence bin. Then, ECE is calculated as follows:

$$\text{ECE} = \sum_{m=1}^M \frac{|B_m|}{N} |Acc(B_m) - Conf(B_m)| \quad (47)$$

$Acc(B_m)$  and  $Conf(B_m)$  are defined as follows

$$Acc(B_m) = \frac{1}{|B_m|} \sum_{b \in B_m} \mathbf{1}(\tilde{y}_b = y_b), \quad Conf(B_m) = \frac{1}{|B_m|} \sum_{b \in B_m} \tilde{p}_b$$

**reliability diagram.** In contrast to ECE, which computes a weighted average, Reliability Diagram calculates an unweighted average.

$$\text{Reliability Diagram} = \sum_{m=1}^M |Acc(B_m) - Conf(B_m)| \quad (48)$$

**mce.** Maximum Calibration Error (MCE) represents the maximum discrepancy between accuracy and confidence across all bins. Formally:

$$\text{MCE} = \max_m |Acc(B_m) - Conf(B_m)| \quad (49)$$

**ace.** It has been pointed out that predictions from recent large-scale models tend to be concentrated in high-confidence ranges (Nixon et al., 2019). Consequently, the equally spaced binning used in ECE results in low-confidence bins containing almost no samples due to this skew. To address this, Adaptive Calibration Error (ACE) (Nixon et al., 2019) dynamically handles confidence bias by partitioning bins to contain an equal number of samples, rather than using equal intervals. Let  $K$  be the number of classes. For each class  $k$ , the prediction confidences are sorted and partitioned into  $M$  subsets of equal size. Let  $B_{m,k}$  denote the  $m$ -th bin for class  $k$ .

$$\text{ACE} = \frac{1}{KM} \sum_{k=1}^K \sum_{m=1}^M |Acc(B_{m,k}) - Conf(B_{m,k})| \quad (50)$$

**temperature scaling.** We calculate the ECE after calibrating the model’s predicted distribution using Temperature Scaling (Guo et al., 2017). Specifically, Temperature Scaling involves dividing the model’s output logits  $z$  by a scalar constant  $T$ . In this study, we determined the optimal  $T$  by minimizing the cross-entropy loss on the training data using the L-BFGS optimizer, and subsequently computed the ECE.

## B. Experiment Setup Details

All experiments were conducted on a single NVIDIA H100 GPU.

### B.1. CIFAR-10

Details of the hyperparameter sweep ranges are provided in Tables 2 and 3. We specified different ranges for the learning rate, as the optimal values vary depending on the optimizer. Additionally, we provided a separate table for NiN, as it is the only architecture that includes width and depth as hyperparameters.

### B.2. DomainBed

The hyperparameter ranges for the DomainBed suites are shown in Table 4 for PACS and VLCS.

Table 2. Hyperparameter search space for SimpleCNN and ResNetV2-32 on CIFAR-10.

Hyperparameter	SGD	RMSProp & Adam
Learning rate	$\{1, 3.2 \times 10^{-1}, 3.2, 1 \times 10^{-2}, 3.2 \times 10^{-3}\}$	$\{1, 3.2 \times 10^{-3}, 1, 3.2 \times 10^{-4}, 3.2 \times 10^{-5}\}$
Batch size		$\{32, 64, 128, 256\}$
Dropout		$\{0, 0.5\}$
Weight decay		$\{0, 1, 5 \times 10^{-4}\}$
Severity of CIFAR-10-C (only in SimpleCNN)		$\{1, 2, 3, 4, 5\}$
Random seed		$\{0, 1, 2, 3, 4\}$

Table 3. Hyperparameter search space for NiN on CIFAR-10.

Hyperparameter	SGD	RMSProp & Adam
Learning rate	$\{1 \times 10^{-1}, 3.2, 1 \times 10^{-2}\}$	$\{1 \times 10^{-3}, 3.2, 1 \times 10^{-4}\}$
Batch size		$\{32, 64, 128\}$
Dropout		$\{0, 0.5\}$
Depth		$\{2, 8\}$
Width		$\{2, 8\}$
Weight decay		$\{0, 5 \times 10^{-4}\}$
Random seed		$\{0, 1, 2, 3, 4\}$

## C. Additional Results

### C.1. Sign-error on CIFAR-10-suite

Here, we present the sign-error results on the CIFAR-10 suite. Fig. 4 shows the results for NiN on CIFAR-10-P, while Fig. 5 and Fig. 6 present the results for SimpleCNN and ResNet across all distributions, respectively.

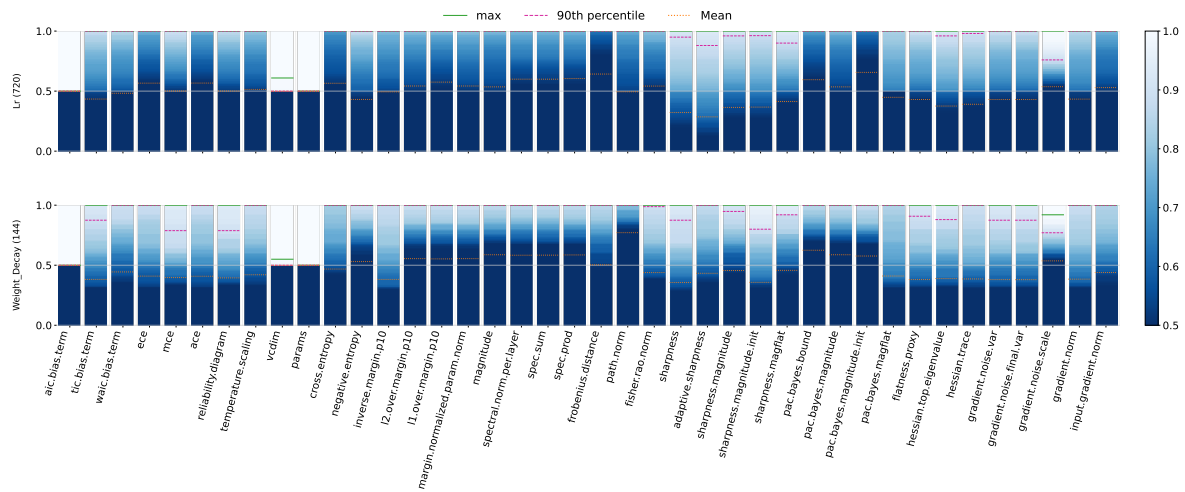


Figure 4. Sign-error distribution of NiN on CIFAR-10-P

Table 4. Hyperparameter search space for PACS and VLCS.

Hyperparameter	
Optimizer	{Adam}
Learning rate	$\{1 \times 10^{-4}, 1, 3, 5 \times 10^{-5}\}$
Batch size	{32}
Weight decay	$\{0, 1 \times 10^{-5}, 1 \times 10^{-4}\}$
Random seed	{0}
Test env idx.	{0, 1, 2, 3}

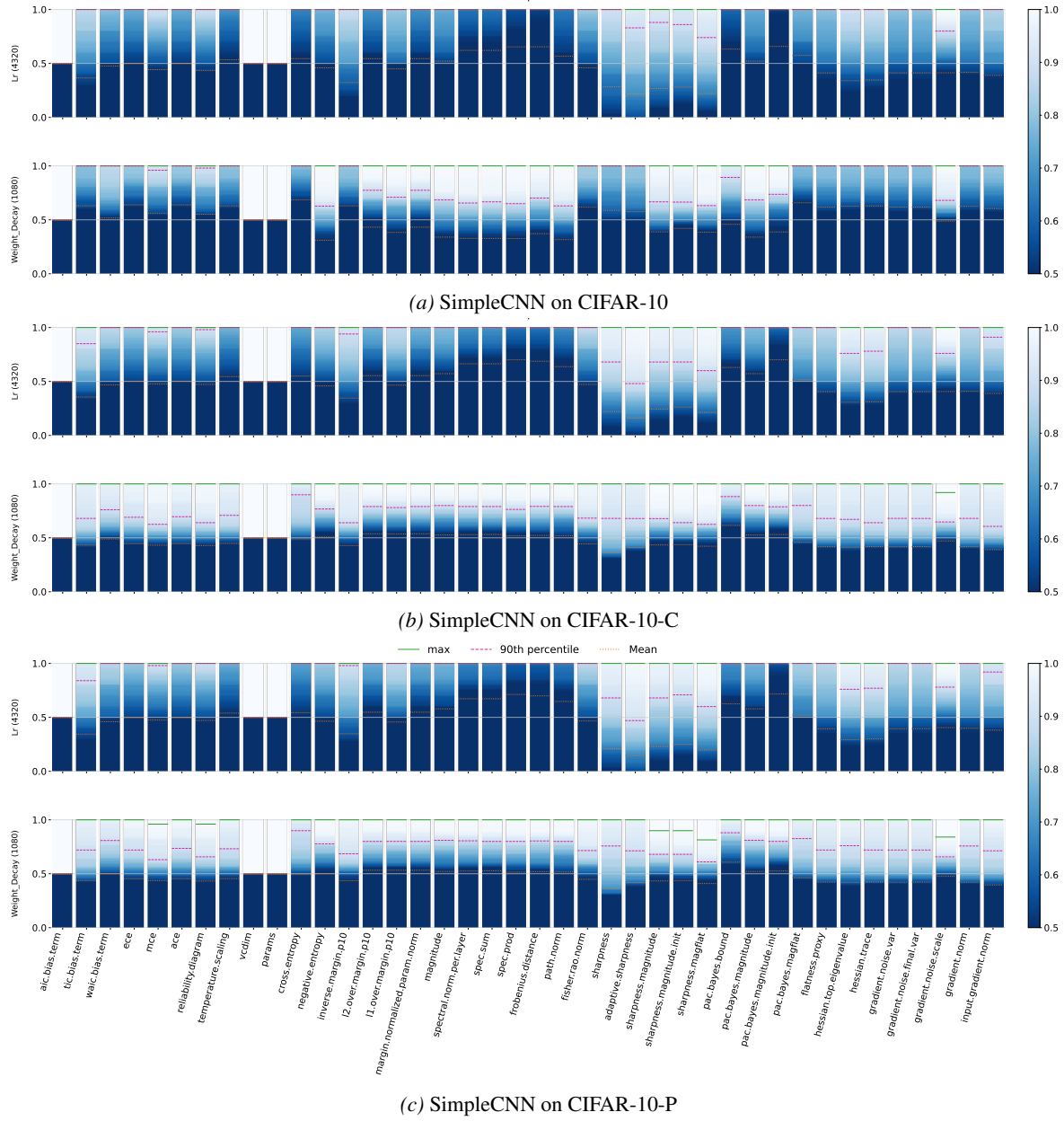


Figure 5. Sign-error distributions of generalization-gap sensitivity for SimpleCNN

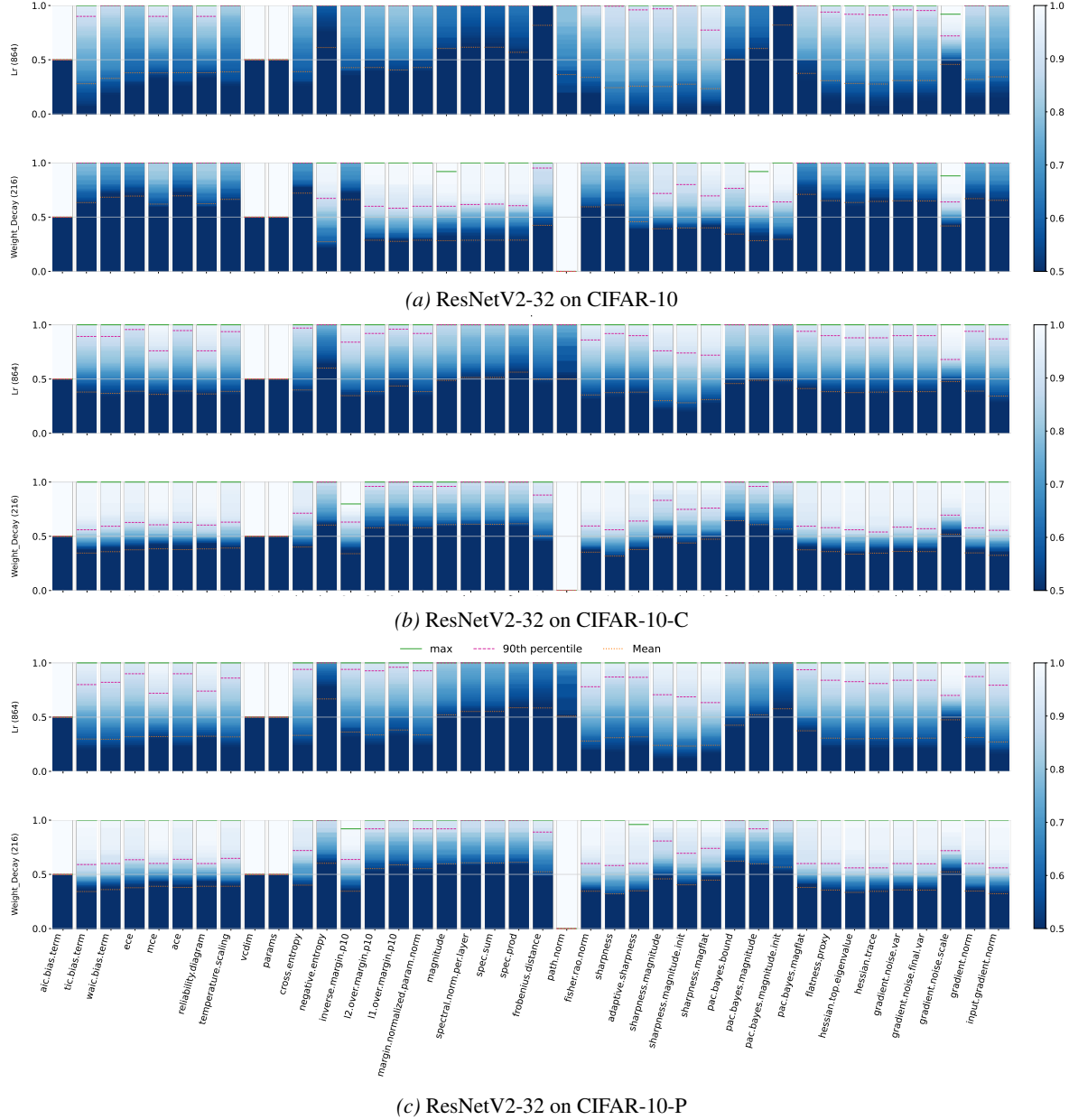


Figure 6. Sign-error distributions of generalization-gap sensitivity for ResNetV2-32

## C.2. Conditional independence Score $K(\mu)$ .

Following [Jiang et al. \(2020\)](#), to account for potential confounding by hyperparameters  $U$ , we assess the conditional dependence between  $\mu$  and  $g$ . We first transform the  $n$  runs into ordered pairs  $(i, j)$  and define ternary sign-difference variables  $V_\mu = \text{sign}(\mu_i - \mu_j)$  and  $V_g = \text{sign}(g_i - g_j)$ . Similarly, for any conditioning subset  $S \subseteq U$ , let  $U_S$  represent the paired hyperparameter values  $(u_i, u_j)$  for  $u \in S$ . We measure the conditional association using normalized conditional mutual information (NCMI):

$$\hat{I}(V_\mu; V_g \mid U_S) = \frac{I(V_\mu; V_g \mid U_S)}{H(V_g \mid U_S)}, \quad (51)$$

where  $I(\cdot | \cdot)$  denotes the discrete conditional mutual information and  $H(\cdot | \cdot)$  is the conditional entropy. The score  $K(\mu)$  is defined as the minimum NCMI over all hyperparameter subsets up to size  $d$ :

$$K(\mu) = \min_{S \subseteq U, |S| \leq d} \widehat{I}(V_\mu; V_g | U_S). \quad (52)$$

A high  $K(\mu)$  indicates that the measure's predictive power is robust and not merely a byproduct of hyperparameter variations. The results are shown in Table 5–10

Table 5. CMI minimum values

Measure	Category	GenGap_CIFAR10	OODGenGap_C	OODGenGap_P
tic_bias_term	Information Criteria	0.0416 (0.0200)	0.0156 (0.0080)	0.0259 (0.0112)
waic_bias_term	Information Criteria	0.0184 (0.0200)	0.0082 (0.0080)	0.0078 (0.0112)
aic_bias_term	Information Criteria	0.0000 (0.0200)	0.0000 (0.0080)	0.0000 (0.0112)

Table 6. CMI minimum values

Measure	Category	GenGap_CIFAR10	OODGenGap_C	OODGenGap_P
temperature_scaling	Calibration & Confidence	0.0214 (0.0137)	0.0051 (0.0098)	0.0071 (0.0117)
mce	Calibration & Confidence	0.0172 (0.0137)	0.0158 (0.0098)	0.0168 (0.0117)
reliability_diagram	Calibration & Confidence	0.0155 (0.0137)	0.0160 (0.0098)	0.0171 (0.0117)
ece	Calibration & Confidence	0.0072 (0.0137)	0.0062 (0.0098)	0.0090 (0.0117)
ace	Calibration & Confidence	0.0072 (0.0137)	0.0059 (0.0098)	0.0087 (0.0117)

Table 7. CMI minimum values

Measure	Category	GenGap_CIFAR10	OODGenGap_C	OODGenGap_P
cross_entropy	Baseline & Output-based	0.0638 (0.0276)	0.0085 (0.0038)	0.0089 (0.0042)
negative_entropy	Baseline & Output-based	0.0464 (0.0276)	0.0069 (0.0038)	0.0079 (0.0042)
params	Baseline & Output-based	0.0000 (0.0276)	0.0000 (0.0038)	0.0000 (0.0042)
vcdim	Baseline & Output-based	0.0000 (0.0276)	0.0000 (0.0038)	0.0000 (0.0042)

Table 8. CMI minimum values

Measure	Category	GenGap_CIFAR10	OODGenGap_C	OODGenGap_P
fisher_rao_norm	Norm & Margin-based	0.0418 (0.0067)	0.0028 (0.0088)	0.0047 (0.0163)
l1_over_margin_p10	Norm & Margin-based	0.0118 (0.0067)	0.0014 (0.0088)	0.0048 (0.0163)
margin_normalized_param_norm	Norm & Margin-based	0.0054 (0.0067)	0.0045 (0.0088)	0.0041 (0.0163)
l2_over_margin_p10	Norm & Margin-based	0.0054 (0.0067)	0.0045 (0.0088)	0.0041 (0.0163)
path_norm	Norm & Margin-based	0.0035 (0.0067)	0.0119 (0.0088)	0.0280 (0.0163)
inverse_margin_p10	Norm & Margin-based	0.0027 (0.0067)	0.0414 (0.0088)	0.0405 (0.0163)
frobenius_distance	Norm & Margin-based	0.0019 (0.0067)	0.0104 (0.0088)	0.0345 (0.0163)
magnitude	Norm & Margin-based	0.0007 (0.0067)	0.0042 (0.0088)	0.0152 (0.0163)
spec_prod	Norm & Margin-based	0.0002 (0.0067)	0.0062 (0.0088)	0.0216 (0.0163)
spectral_norm_per_layer	Norm & Margin-based	0.0002 (0.0067)	0.0016 (0.0088)	0.0025 (0.0163)
spec_sum	Norm & Margin-based	0.0001 (0.0067)	0.0075 (0.0088)	0.0195 (0.0163)

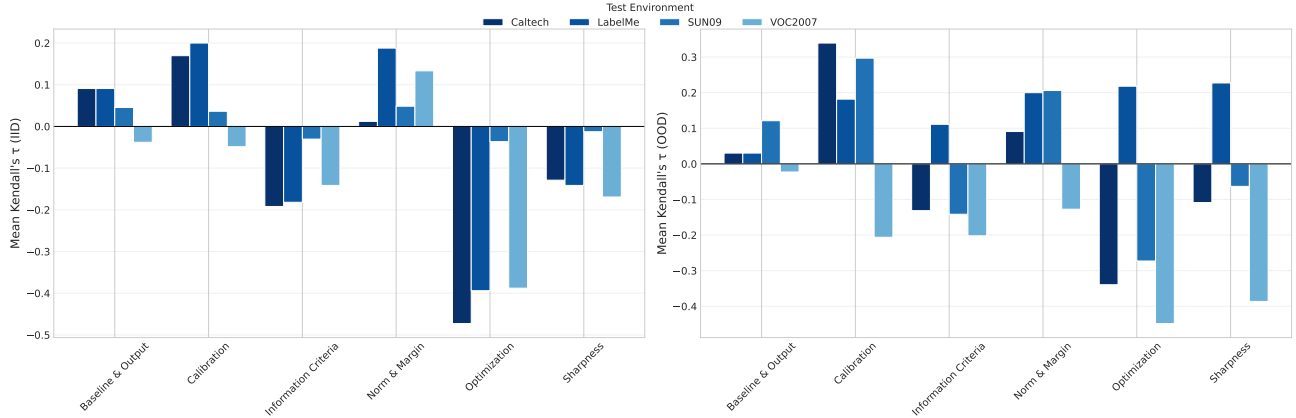
Table 9. CMI minimum values

Measure	Category	GenGap_CIFAR10	OODGenGap_C	OODGenGap_P
hessian_top_eigenvalue	Sharpness-based	0.0324 (0.0089)	0.0235 (0.0155)	0.0465 (0.0313)
hessian_trace	Sharpness-based	0.0309 (0.0089)	0.0207 (0.0155)	0.0424 (0.0313)
flatness_proxy	Sharpness-based	0.0234 (0.0089)	0.0171 (0.0155)	0.0252 (0.0313)
sharpness	Sharpness-based	0.0078 (0.0089)	0.0384 (0.0155)	0.0612 (0.0313)
pac_bayes_bound	Sharpness-based	0.0064 (0.0089)	0.0045 (0.0155)	0.0121 (0.0313)
sharpness_magflat	Sharpness-based	0.0021 (0.0089)	0.0094 (0.0155)	0.0296 (0.0313)
adaptive_sharpness	Sharpness-based	0.0011 (0.0089)	0.0455 (0.0155)	0.0742 (0.0313)
pac_bayes_magflat	Sharpness-based	0.0011 (0.0089)	0.0086 (0.0155)	0.0060 (0.0313)
sharpness_magnitude_init	Sharpness-based	0.0010 (0.0089)	0.0074 (0.0155)	0.0310 (0.0313)
pac_bayes_magnitude	Sharpness-based	0.0007 (0.0089)	0.0042 (0.0155)	0.0152 (0.0313)
pac_bayes_magnitude_init	Sharpness-based	0.0002 (0.0089)	0.0000 (0.0155)	0.0003 (0.0313)
sharpness_magnitude	Sharpness-based	0.0000 (0.0089)	0.0067 (0.0155)	0.0320 (0.0313)

Table 10. CMI minimum values

Measure	Category	GenGap_CIFAR10	OODGenGap_C	OODGenGap_P
gradient_norm	Optimization-based	0.0381 (0.0242)	0.0146 (0.0117)	0.0248 (0.0188)
gradient_noise_var	Optimization-based	0.0365 (0.0242)	0.0145 (0.0117)	0.0246 (0.0188)
gradient_noise_final_var	Optimization-based	0.0269 (0.0242)	0.0171 (0.0117)	0.0267 (0.0188)
input_gradient_norm	Optimization-based	0.0194 (0.0242)	0.0095 (0.0117)	0.0110 (0.0188)
gradient_noise_scale	Optimization-based	0.0001 (0.0242)	0.0030 (0.0117)	0.0072 (0.0188)

### C.3. DomainBed-suite


 Figure 7. Mean Kendall's  $\tau$  for measure families across VLCS environments.

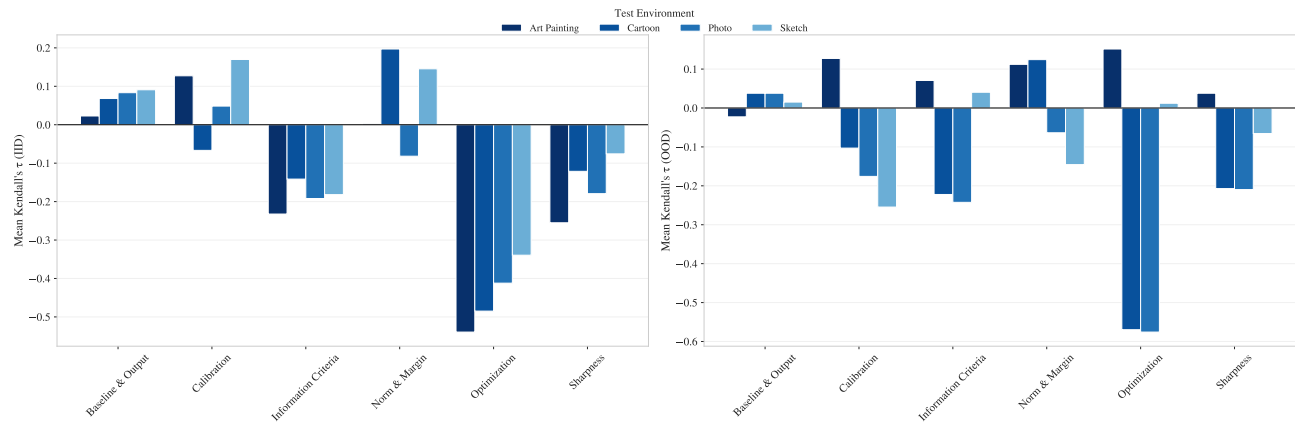


Figure 8. Mean Kendall's  $\tau$  for measure families across PACS environments.

## Revisiting Generalization Measures Beyond IID

*Table 11.* PACS summary of IID/OOD correlations and hyperparameter sensitivities for each measure.

Measure	$lr^{IID}$	$lr^{OOD}$	$wd^{IID}$	$wd^{OOD}$	$\tau^{IID}$	$\tau^{OOD}$	$\Psi^{IID}$	$\Psi^{OOD}$
gradient.noise.var	-0.7222	-0.3889	-0.0833	-0.3333	-0.6364	-0.3258	-0.4028	-0.3611
hessian.top.eigenvalue	-0.6389	-0.3611	-0.0833	-0.0833	-0.5530	-0.3182	-0.3611	-0.2222
input.gradient.norm	-0.4167	-0.3611	0.0417	-0.0417	-0.4167	-0.3182	-0.1875	-0.2014
gradient.noise.final.var	-0.5556	-0.2778	0.1667	-0.0833	-0.4924	-0.3030	-0.1944	-0.1806
hessian.trace	-0.4722	-0.3611	0.0000	0.0000	-0.4015	-0.2727	-0.2361	-0.1806
pac.bayes.magnitude.init	0.8333	0.3333	-0.0417	0.0417	0.6667	0.2652	0.3958	0.1875
tic.bias.term	-0.7222	-0.2778	0.1667	-0.0833	-0.5606	-0.2652	-0.2778	-0.1806
gradient.norm	-0.7222	-0.3333	0.1667	0.0833	-0.5909	-0.2500	-0.2778	-0.1250
frobenius.distance	0.8333	0.3333	-0.0833	-0.0000	0.5530	0.2273	0.3750	0.1667
sharpness.magflat	-0.5833	-0.3056	-0.1667	0.0833	-0.5076	-0.2273	-0.3750	-0.1111
ace	0.0000	-0.2222	0.1667	-0.1667	-0.0455	-0.2045	0.0833	-0.1944
flatness.proxy	-0.7778	-0.2778	-0.0417	0.1250	-0.6364	-0.2045	-0.4097	-0.0764
sharpness.magnitude	-0.3333	-0.1667	-0.0417	-0.1250	-0.2955	-0.1970	-0.1875	-0.1458
ece	-0.0556	-0.1667	0.1667	-0.0833	0.0303	-0.1894	0.0556	-0.1250
path.norm	-0.7222	-0.3889	0.0833	0.0000	-0.2273	-0.1742	-0.3194	-0.1944
fisher.rao.norm	-0.0833	-0.1389	0.2500	-0.0833	-0.0758	-0.1591	0.0833	-0.1111
temperature.scaling	0.1944	-0.0833	0.2500	-0.1667	0.1212	-0.1439	0.2222	-0.1250
sharpness	-0.4167	-0.1389	-0.0417	0.0417	-0.3106	-0.1212	-0.2292	-0.0486
pac.bayes.magnitude	-0.2778	-0.2222	0.0833	0.0000	-0.0530	-0.1061	-0.0972	-0.1111
magnitude	-0.2778	-0.2222	0.0833	0.0000	-0.0530	-0.1061	-0.0972	-0.1111
adaptive.sharpness	0.2222	0.1667	0.2083	0.0417	0.3106	0.0909	0.2153	0.1042
spectral.norm.per.layer	0.1111	0.1111	0.0833	0.0000	0.1515	0.0833	0.0972	0.0556
spec.sum	0.1111	0.1111	0.0833	0.0000	0.1515	0.0833	0.0972	0.0556
spec.prod	0.1667	0.1111	0.0833	0.0000	0.2197	0.0758	0.1250	0.0556
pac.bayes.bound	0.0278	-0.0833	0.0000	-0.0833	0.1061	-0.0682	0.0139	-0.0833
margin.normalized.param.norm	-0.1389	-0.0278	-0.0833	-0.0833	-0.1212	-0.0682	-0.1111	-0.0556
pac.bayes.magflat	-0.1667	-0.1111	-0.0833	-0.0000	-0.1667	-0.0682	-0.1250	-0.0556
mce	0.2222	0.0000	-0.0833	-0.0000	0.1591	0.0606	0.0694	-0.0000
inverse.margin.p10	0.0000	-0.0000	0.1667	0.0833	0.0379	0.0606	0.0833	0.0417
l2.over.margin.p10	-0.0278	-0.0278	0.1667	0.0833	-0.0606	-0.0379	0.0694	0.0278
negative.entropy	0.0833	0.0833	0.1250	-0.1250	0.1061	0.0379	0.1042	-0.0208
reliability.diagram	0.1667	0.0000	0.0000	-0.0833	0.0833	-0.0303	0.0833	-0.0417
cross.entropy	0.1389	-0.0278	0.2500	0.0833	0.1591	0.0303	0.1944	0.0278
gradient.noise.scale	-0.1667	-0.1111	0.0833	0.0000	-0.0833	-0.0303	-0.0417	-0.0556
l1.over.margin.p10	0.1111	0.0556	-0.0417	-0.0417	0.0303	-0.0227	0.0347	0.0069
aic.bias.term	0.0000	0.0000	0.0000	0.0000	0.0000	0.0000	0.0000	0.0000
params	0.0000	0.0000	0.0000	0.0000	0.0000	0.0000	0.0000	0.0000
vcdim	0.0000	0.0000	0.0000	0.0000	0.0000	0.0000	0.0000	0.0000
waic.bias.term	0.0000	0.0000	0.0000	0.0000	0.0000	0.0000	0.0000	0.0000

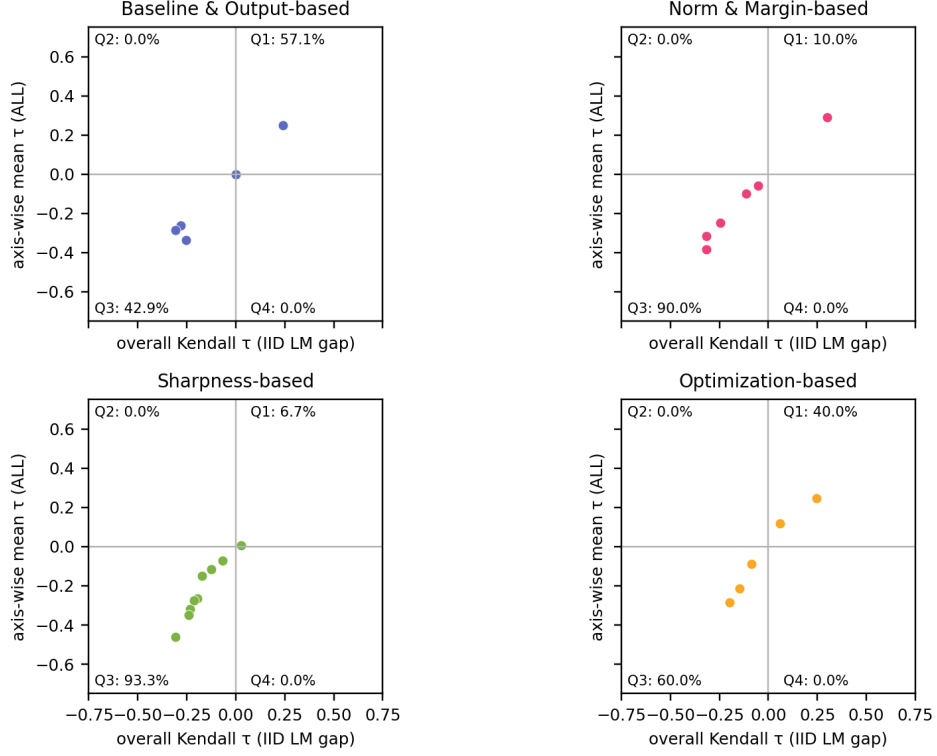
Table 12. VLCS summary of IID/OOD correlations and hyperparameter sensitivities for each measure.

Measure	$lr^{IID}$	$lr^{OOD}$	$wd^{IID}$	$wd^{OOD}$	$\tau^{IID}$	$\tau^{OOD}$	$\Psi^{IID}$	$\Psi^{OOD}$
frobenius.distance	0.5000	0.5000	0.0000	-0.0417	0.4091	0.3182	0.2500	0.2292
hessian.top.eigenvalue	-0.3333	-0.3889	-0.0417	-0.1667	-0.3182	-0.3182	-0.1875	-0.2778
hessian.trace	-0.3889	-0.4444	0.0417	0.0000	-0.3712	-0.3106	-0.1736	-0.2222
gradient.noise.var	-0.5000	-0.5000	0.0833	0.2083	-0.4091	-0.3030	-0.2083	-0.1458
flatness.proxy	-0.5000	-0.5000	0.1250	0.3333	-0.3939	-0.3030	-0.1875	-0.0833
pac.bayes.magnitude.init	0.5000	0.5000	-0.0417	-0.3333	0.4545	0.3030	0.2292	0.0833
gradient.norm	-0.4444	-0.5000	0.1250	0.3333	-0.4015	-0.2955	-0.1597	-0.0833
gradient.noise.final.var	-0.3333	-0.5000	0.1250	0.1667	-0.3182	-0.2879	-0.1042	-0.1667
tic.bias.term	-0.4444	-0.5000	-0.0833	0.2917	-0.4091	-0.2727	-0.2639	-0.1042
input.gradient.norm	-0.4444	-0.4444	0.0000	0.4583	-0.3409	-0.2045	-0.2222	0.0069
pac.bayes.magflat	-0.1389	-0.1944	0.0000	-0.0417	-0.1439	-0.2045	-0.0694	-0.1181
spec.sum	0.1111	0.1667	-0.0000	0.0417	0.1439	0.1894	0.0556	0.1042
mce	0.1944	0.1389	0.0417	0.0833	0.1894	0.1894	0.1181	0.1111
spectral.norm.per.layer	0.1111	0.1667	-0.0000	0.0417	0.1364	0.1818	0.0556	0.1042
sharpness.magflat	-0.2778	-0.2778	0.1667	0.2083	-0.1667	-0.1818	-0.0556	-0.0347
spec.prod	0.1389	0.1944	-0.0000	0.0417	0.1818	0.1818	0.0694	0.1181
reliability.diagram	0.1389	0.3056	0.0000	0.1250	0.1742	0.1742	0.0694	0.2153
negative.entropy	0.2500	0.1944	-0.2083	0.0000	0.1667	0.1667	0.0208	0.0972
ace	0.0833	0.1944	0.0833	0.1250	0.0076	0.1439	0.0833	0.1597
temperature.scaling	0.0556	0.0556	0.1250	0.3333	0.0152	0.1364	0.0903	0.1944
ece	0.1389	0.1389	0.2083	0.2500	0.0606	0.1212	0.1736	0.1944
path.norm	0.0556	0.0556	-0.0000	0.0417	0.0758	0.1212	0.0278	0.0486
adaptive.sharpness	0.2222	0.0000	0.2500	0.2083	0.1818	0.1212	0.2361	0.1042
sharpness.magnitude	-0.3333	-0.3333	0.0000	0.0417	-0.2424	-0.1212	-0.1667	-0.1458
sharpness	-0.4444	-0.2778	0.2917	0.1667	-0.2727	-0.1061	-0.0764	-0.0556
magnitude	-0.0556	-0.0556	-0.0000	0.0417	-0.0303	0.0758	-0.0278	-0.0069
pac.bayes.magnitude	-0.0556	-0.0556	-0.0000	0.0417	-0.0303	0.0758	-0.0278	-0.0069
fisher.rao.norm	0.1389	-0.0833	0.3333	0.1250	0.1136	-0.0682	0.2361	0.0208
inverse.margin.p10	0.0556	0.1667	0.2917	-0.0000	0.1136	0.0682	0.1736	0.0833
gradient.noise.scale	-0.1667	-0.1111	-0.2083	0.1667	-0.1439	0.0379	-0.1875	0.0278
margin.normalized.param.norm	-0.1111	0.0556	0.0833	0.2083	-0.0833	-0.0379	-0.0139	0.1319
pac.bayes.bound	-0.0278	-0.0278	0.0000	0.2083	-0.0227	-0.0227	-0.0139	0.0903
l2.over.margin.p10	-0.1389	-0.0278	0.1667	0.2917	-0.0758	-0.0152	0.0139	0.1319
l1.over.margin.p10	-0.0556	0.0556	0.0417	0.0833	-0.0606	-0.0152	-0.0069	0.0694
cross.entropy	0.0556	0.0000	0.0417	0.1667	0.0227	-0.0076	0.0486	0.0833
aic.bias.term	0.0000	0.0000	0.0000	0.0000	0.0000	0.0000	0.0000	0.0000
params	0.0000	0.0000	0.0000	0.0000	0.0000	0.0000	0.0000	0.0000
vcdim	0.0000	0.0000	0.0000	0.0000	0.0000	0.0000	0.0000	0.0000
waic.bias.term	0.0000	0.0000	0.0000	0.0000	0.0000	0.0000	0.0000	0.0000

#### C.4. DistilGPT2

All experiments were conducted on eight NVIDIA V100 GPUs. We included a small language-modeling experiment to assess whether the qualitative behavior of generalization measures transfers beyond vision. We swept a single architecture (DistilGPT2) on Wikitext-103 (train/validation) and computed Kendall’s  $\tau$  between each measure and the IID generalization gap. This appendix is IID-only and single-architecture, so our results are not intended as evidence of OOD robustness or stability.

**Overall Kendall’s  $\tau$  (IID LM gap).** The strongest absolute correlations are modest ( $|\tau| \approx 0.30$ ). Representative top- $|\tau|$  measures and capacity baselines are shown in Figure 9.

LM sanity-check: overall  $\tau$  vs axis-wise mean  $\tau$ 

 Figure 9. Overall Kendall's  $\tau$  between each measure and the IID generalization gap for DistilGPT2 on Wikitext-103.

**Axis sensitivity (sign flips across learning rate / batch size).** Axis-wise mean Kendall's  $\tau$  (computed by fixing all other hyperparameters and varying one axis) shows pronounced sign changes for several measures, indicating hyperparameter dependence even in IID LM settings.

Table 13. Axis-wise mean Kendall's  $\tau$  with the IID generalization gap for selected measures. Sign flips indicate strong dependence on the training axis even in IID.

Measure	Learning rate ( $\bar{\tau}_{lr}$ )	Batch size ( $\bar{\tau}_{batch}$ )
Cross-entropy	+0.364	-0.571
Negative entropy	-0.493	+0.667
Inverse margin (p10)	+0.450	-0.726